Functional characterization of PTCHD1, a risk gene for autism spectrum disorders and intellectual disabilities

Inauguraldissertation
zur
Erlangung der Würde eines Doktors der Philosophie
vorgelegt der
Philosophisch-Naturwissenschaftlichen Fakultät
der Universität Basel

von

David Tora
Frankreich & Ungarn.

Basel, 2019.

Philosophisch-Naturwissenschaftlichen Fakultät
auf Antrag von:

Prof. Dr. Peter Scheiffele

Prof. Dr. Silvia Arber

Basel, den 26.06.2018

Prof. Dr. Martin Spiess
Dekan der Philosophisch-
Naturwissenschaftlichen Fakultät

Table of content

Summary

Autism spectrum disorders (ASD) are lifelong severe disabling conditions affecting around 1-2% of the global population (Elsabbagh et al., 2012; Baxter et al., 2015; Christensen et al., 2016). In the past decade, improvements in whole genome sequencing methods allowed the identification of increasing numbers of risk genes associated with ASD. Studies suggest that risk genes converge in several common molecular, metabolic, or circuit pathways (de la Torre-Ubieta et al., 2016). Despite these recent advances in the biological understanding of ASD, no efficient treatments have been found yet. Therefore, identifying the function of individual genes leading to converging alterations is a major challenge to define mechanism based stratification of the disorder.

The goal of my study was to explore the functions of the Patched domain containing protein 1, a poorly understood risk gene strongly associated with ASD and intellectual disability (ID) (Noor et al., 2010; Chaudhry et al., 2015). PTCHD1 appears to be a highly penetrant mutation with around 45% of affected individuals having ASD and/or ID (Chaudhry et al., 2015). It is estimated that mutations in the PTCHD1 locus occur in approximately 1% of individuals with ASD (Noor et al., 2010). Thus, compared to other genetic risk factors, PTCHD1 mutation appear to be a common and very penetrant alteration associated with ASD. To date the Ptchd1 protein has remained largely uncharacterized, therefore, there is a lack of insights into how PTCHD1 mutations may lead to ASD related phenotypes. The gene encodes for a transmembrane protein that shares a sterol-sensing domain with the Sonic hedgehog (Shh) receptor Patched (Ptch1) and Niemann-Pick disease, type C1 (NPC1), a cholesterol transport protein. Based on this sequence similarity and transcriptional reporter assays in cell lines, it has been hypothesized that Ptchd1 may contribute to Shh signaling (Noor et al., 2010).

Here I report, using a mouse knock-out model and biochemical assays, that Ptchd1 removal has no effect on Shh dependent neuronal proliferation, in addition, Shh does not show any binding to Ptchd1 *in vitro*. In an unbiased search for Ptchd1 interacting proteins, I recovered three components of the retromer complex involved in regulating dendritic protein trafficking between endosomal compartments and the plasma membrane (Choy et al., 2014): Sorting-nexin 27, VPS26B and VPS35. In addition, several postsynaptic density proteins were recovered: Dlg1,2,3,4 Magi1,3, Lin7. Considering a potential synaptic role for Ptchd1, we performed electrophysiological recordings on Ptchd1 knock-out animals in granule cells of the dentate gyrus, a cell population where Ptchd1 is highly enriched. We observed that loss of Ptchd1 results in a disruption of excitatory/inhibitory balance in the mouse hippocampus. Finally, Ptchd1 KO animals also showed deficits in hippocampus-related behavioral tasks.

Thereby, my study provides evidence that Ptchd1 loss-of-function experiments do not support a role in sonic-hedgehog-dependent signaling but reveal a profound disruption of synaptic transmission in the mouse dentate gyrus and support an association of Ptchd1 with dendritic trafficking complexes and synaptic scaffolding proteins.

1. Introduction

1.1 General introduction

The development of the brain is orchestrated by complex genetic programs defining distinct and specific cellular functions. The resulting cellular and molecular diversity aims to build an efficient neuronal network but the correct functioning of the brain is a fragile balance where a single genetic mutation can induce severe neurodevelopmental disorders. Thereby, understanding how genetic mutations lead to complex neurodevelopmental disorders is a major challenge for neurobiologists. Mutations can affect specific brain functions such as cognitive, emotional, learning, social or motor processing but they often result in a combination of phenotypic alterations. In the past decades, several neurodevelopmental conditions have been linked with rare genetic mutations such as Fragile X, Tuberous sclerosis or Rett syndrome. However, in most cases developmental brain alterations arise from a combination of multi-genic and environmental factors often leading to complex and severe conditions such as autism spectrum disorders (ASD), schizophrenia or bipolar disorders. ASD appears to be the most prevalent of neurodevelopmental disorders with around 1-2% of the global population affected (Elsabbagh et al., 2012; Baxter et al., 2015; Christensen et al., 2016). In the past decade, there has been a converging line of research, especially twin studies and sequencing studies, suggesting that ASD has a strong genetic component (Folstein and Rutter, 1977a; Ronald and Hoekstra, 2011; Geschwind and State, 2015) . With the improvement of genome wide sequencing methods, more than a hundred of risk genes have been identified and the list is constantly increasing (Geschwind and State, 2015). A great number of risk genes are suggested to converge in common molecular, cellular or metabolic pathways (de la Torre-Ubieta et al., 2016). However the link between gene mutation and altered phenotype is, in most cases not elucidated. In addition, with new risk genes constantly added to the list, a great number of them stay unstudied.

Thus, the pathophysiology of ASD remains poorly understood with no clear therapeutic targets identified. Thereby disentangling the genetics of ASD is essential to establish a mechanism-based stratification of different ASD forms and thereby provide targeted molecular therapies.

1.2 Autism spectrum disorders: a single condition?

1.2.1 A historical perspective

In the late 1800s, a period when interest towards mental illness was starting to emerge, the term “autism”, from the Greek word “autos” meaning “self”, was first reported by Dr. John Langdon describing the “autistic thinking” of patients having Down’s syndrome. At the time, the term “autistic” was referring to a person who is “cut off the world of people”. Later in the early 1900s Eugen Bleuler and his student Eugène Minkowski, used the term autism to describe symptoms of what they called “dementia praecox” (early psychosis) later named childhood schizophrenia. In both cases, the word autism did not yet refer to the current definition, but rather a simplistic description of mental retardation.

In the 1940s that Leo Kanner (Johns Hopkins Hospital, United States) and Hans Asperger (University of Vienna, Austria) conducted in parallel similar observations on children and characterized for the first time patients having difficulties to deal with social interaction and communication. Even though both practitioners described similar observation around the same period, Leo Kanner documented more carefully his observations and identified children’s difficulties to deal with non-social changes and was the first to use the concepts of “resistance to change” and “insistence on sameness”. In addition he also distinguished autism from mental retardation and described some of the affected children as “feeble minded”. Leo Kanner and Hans Asperger’s observations were close to the current definition of ASD, however it was not yet considered as a separate disorder and the confusion with mental retardation and “childhood schizophrenia” still remained.

After the second world war many child psychiatrists were still diagnosing children presenting social deficits/repetitive behaviors with child schizophrenia, often interpreting its origin in psychoanalytic terms. An interpretation that gained a lot of attention at the time, was that the condition is a form a rejection of reality in response to an emotionally cold and distant mother (also known as the “refrigerator mother” theory). Parental education being a cause for autism was a popular theory in the 1960s, mainly because some psychiatrists reported that most of the affected children came from highly educated families; which led

practitioners to conclude that autism was specific to high-status families and deviant parenting could be a cause of autism. However, it was without considering the selection bias that well informed and educated families have more chance to find a psychiatrist and diagnose their child. Thus, several child psychiatrists later focused on the question and found no link between parental education and ASD (Rutter, 1979) .

It is only in the early 1970s that the biological origin of ASD started to emerge with the establishment of precise clinical models and epidemiological studies. Pioneering studies led by Michael Rutter suggested that ASD and schizophrenia were genetically dissociated by showing that patients with ASD did not have increased rates of schizophrenia compared to the general population (Rutter, 1972). Similarly, Israel Kolvin's established that ASD and schizophrenia had independent developmental trajectories and different ages of onset (Kolvin, 1971). From that point onwards, clinicians defined a more detailed diagnostic model, including the early onset (within 30 months of age) of social interaction deficits, behavioral rigidities, hyper/hyposensitivity to the environment and language deficit or absence of speech.

In the late 1970s Susan Folstein and Michael Rutter conducted the first studies comparing twins with either one or both having autism. The studies concluded that there was a very high concordance rate for autism between twins and thereby highlighted for the first time the heritability of autism (Folstein and Rutter, 1977b).These converging studies strongly contributed to recognize "infantile autism" as a separate diagnosis in the third edition of Diagnostic and Statistical Manual of Mental Disorders (DSM-III) in 1980.

In 1987, the term "infantile autism" was renamed to "autism disorder" with the aim to orient the diagnosis to a broader developmental approach (not only limited to young children). Thereby some major changes were made to the definition of the diagnosis in the revision of the DSM-III (DSM-III-R); sixteen criteria were established within three major groups of dysfunctions: (1) qualitative impairment in reciprocal social interaction, (Andersen and Koeppe) qualitative impairment in communication and (3) restricted interests. Eight criteria out of sixteen had to be met to diagnose autism disorder, with at least two from the social category and one each from the other two categories. This detailed diagnostic scheme gave

more flexibility to clinicians for establishing an accurate diagnosis and focused more on the behavioral changes during development. However, the early onset of the disorder was often missed and gave a significant number of false positive cases, mainly patients with intellectual disability.

In the 1990s a series of field trial compared different version of diagnostic schemes including DSM-III, DSM-III-R and the World Health Organization's International Statistical Classification of Diseases and Related Health Problems (ICD-10). In 1994, after multiple analysis comparing the diagnostic schemes, a new class of subthreshold condition of autism was added to the DSM-IV. In other words, patients meeting some but not full autism diagnostic criteria were categorized under the "pervasive developmental disorders" (PDD) category also referred as "atypical autism" in the ICD-10. This category included "childhood disintegrative disorder", Rett syndrome (a genetic disorder including social impairment and severe motor dysfunctions) and Asperger syndrome (patients with social deficits but no impairment in communication and normal or higher than average cognitive functions).

Finally in 2013, the fifth edition of the DSM adopted the term "autism spectrum disorder" with the aim to better define the different dimensions of the disorder not only for clinical but also for neurobiological purposes. The current definition merges impairment in social interaction and communication in one group, but kept restricted and repetitive behaviors as a second core feature. The term "spectrum" replaces the PDD terminology and aims to highlight the variety and complexity of comorbid disorders associated with the core symptoms.

In sum, since the early 1800s there has been a considerable effort to shape the definition of ASD. First, it helped to recognize and define the disorder as a separate and complex condition, then guided clinicians to make an accurate diagnostic with the aim to provide adapted care to patients.

1.2.2 Distinction between core and associated symptoms

To meet full ASD diagnosis according to the DSM-V, a person must show deficits in all features of the social interaction/communication category:

1. Social-emotional reciprocity
2. Non-verbal communication
3. Understanding and maintaining relationships.

In addition, the person must demonstrate deficits in two out four features in the restricted/repetitive behaviors cluster:

1. Repetitive speech/behavior
2. Insistence on sameness
3. Restricted interests
4. Sensory abnormalities.

Deficits in social interaction/communication and restricted/repetitive behaviors currently define the two core symptoms of ASD, however the disorder is often accompanied by several comorbidities that shape a heterogeneous and complex spectrum. Associated symptoms are often reported to be more disabling on a daily bases than the core symptoms. As illustrated in Figure 1, comorbidities are very heterogeneous and can affect cognitive, behavioral as well as more autonomous functions such as the gastrointestinal tract and sleep rhythms.

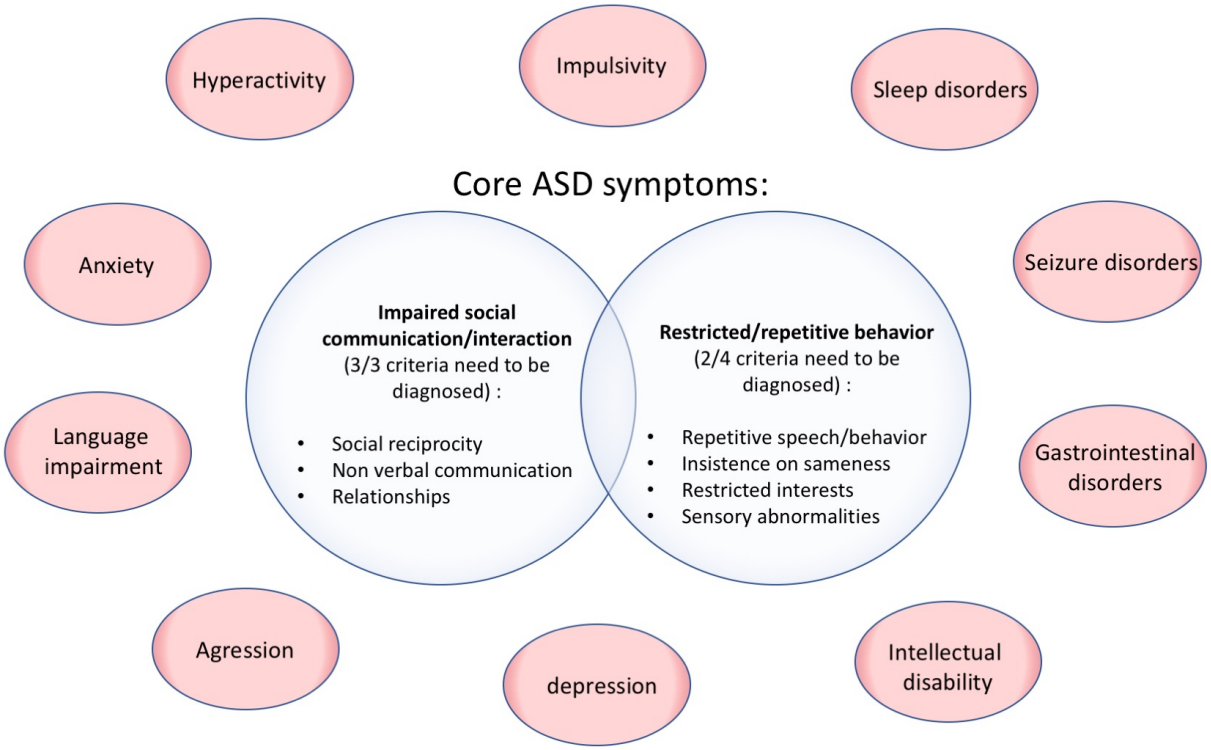

Figure 1. Heterogeneity of ASD comorbidities. Adapted from Veenstra-VanderWeele and Blakely (2012). Core symptoms are described in blue circles. Comorbidities are shown in red circles. Associated symptoms can be behavioral such as hyperactivity, impulsivity, anxiety, aggression, depression; or/and cognitive: intellectual disability, language impairment; and/or medical: sleep, gastrointestinal, seizure disorders.

Within the ASD behavioral comorbidities, intellectual disability (ID) appears to be the most frequent, with approximately 1/3 of patient being affected (Chakrabarti and Fombonne, 2005; Fombonne, 2009; Postorino et al., 2016). Diagnosis of ID involves several test such as intellectual functioning (IQ tests) and emotional/social maturity, however the evaluation methods can differ across countries which makes epidemiologic studies difficult to establish. In addition, self-injury and aggression are also commonly observed in individuals with ID. The debate remains on whether or not emotional/social interaction disorders can be a cause of ID; in other words when ASD is diagnosed with ID, the core symptoms of impaired social communication/ interaction could be a consequence of ID and not a core feature anymore.

Anxiety disorders are also commonly diagnosed with ASD and often observed when the repetitive routine is changed and/or an unexpected or novel task has to be initiated. However it remain unclear whether or not the anxiety state causes the repetitive disorders or if the restricted/repetitive rigidity create the anxiety towards change/novelty or unexpected events.

Within the medical comorbidities, epilepsy is often an early sign leading to the detection of ASD with around 20-30% of individuals affected (Francis et al., 2013; Viscidi et al., 2013). It has been hypothesized that epilepsy could play a role in regressive ASD (individuals loosing acquired skills during preschool period including language, social skills, etc.). However, current studies do not support a strong correlation (Tuchman, 2006; Besag, 2018).

Overall, the comorbid symptoms discussed above are more likely to occur in individuals with ASD compared to typically developing persons (Elsabbagh et al., 2012), and for most of the comorbidities it is still debated whether they are a cause or a consequence of the core symptoms. With the complexity and heterogeneity of core and associated symptoms each individual with ASD is a unique case and therefore needs careful diagnosis and adapted care. Over the past decade, considerable efforts have been made to create diagnostic tools to identify and dissociate core from associated symptoms. Standardized diagnosis tools are important to identify and treat comorbidities when medications or therapies are available. However standardization also has limitations, diagnosing one dysfunction (for example ID) may lead to miss the identification of more subtle dysfunctions (mental illness,

communication impairment, physical pain, etc.), called “diagnostic overshadowing”. Also, attributing a multitude of symptoms, often negatively seen by the society, to an individual with ASD can also be very stigmatizing and worsen the symptoms.

Some comorbidities can be attenuated with medication (hyperactivity, anxiety, aggression, sleep) but are often accompanied by undesired side effects. Behavioral therapies can improve to various degrees some of the core symptoms but are inefficient in many cases. Overall, there is currently no adequate treatment targeting the core symptoms, mainly because the biological understanding of ASD just started to emerge. Since researchers started investigating the comorbidities on a biological level, it raised the question on whether different ASD symptoms arise from a single underlying etiology or whether different biological deficits cause converging ASD symptoms. Over the past decade, the improvement of research tools (brain imaging, cell imaging and molecular biology tools) provided elements of response with the identification of several biological alterations.

1.2.3 Biological deficits

Understanding the pathophysiology of ASD is an essential step toward the development of specific molecular therapies. Recent studies reported biological dysfunctions at various levels including anatomical, circuit, cellular and/or molecular levels (de la Torre-Ubieta et al., 2016). This section highlight the principal biological alterations identified so far.

Anatomical alterations often include brain overgrowth during early child hood that either can persist over time or be followed by a growth normalization during development. Abnormal head circumference (macrocephaly or microcephaly) is also observed in approximately 20% of children with ASD (Fombonne et al., 1999). Not all brain regions are affected by an overgrowth pattern but the frontal lobes and anterior temporal regions, involved in processing language and social cognition (Amaral et al., 2008) appear to be the most affected (Courchesne et al., 2007).

Growth alterations also suggest underlying circuit deficits. Altered functional connectivity with disruptions in short and long-range connections is strongly associated with

ASD. Studies report either under or over-connectivity in both local and long-range connections (Courchesne and Pierce, 2005; Anderson et al., 2011; Keown et al., 2013). Several studies from human derived cells and mouse models, report alterations in excitatory (E) or inhibitory (I) circuits, which led to the hypothesis that an imbalance of excitation over inhibition (E/I ratio) contributes to ASD pathophysiology (Shcheglovitov et al., 2013; Nelson and Valakh, 2015; Patriarchi et al., 2016).

Connectivity can be also structurally altered in ASD, with disruptions in neuronal cytoarchitecture. Post-mortem brains of ASD patients and mouse models showed alterations in neuronal density, size and localization (Casanova et al., 2002; Casanova et al., 2006)

Excitatory and inhibitory neurotransmission is processed by synapses and malfunctioning synapses are thought to be strongly contributing to ASD (Kleijer et al., 2014; Ebrahimi-Fakhari and Sahin, 2015). Several genes encoding for synaptic proteins have been closely linked with ASD : Synaptic adhesion molecules (neurexins, neuroligins) (Jamain et al., 2003; Vaags et al., 2012; De Rubeis et al., 2014), Synaptic scaffolding proteins (SHANKs, Gephyrins) (Durand et al., 2007; Berkel et al., 2010; Lionel et al., 2013) and post-synaptic receptors (GABA and NMDA) (De Rubeis et al., 2014; Krumm et al., 2015). Synaptic dysfunction in ASD also includes altered synaptogenesis (Garcia-Penas et al., 2012; Habela et al., 2016) and synaptic pruning deficits (Hutsler and Zhang, 2010; Tang et al., 2014).

Deficits in neuronal translation are also associated with ASD. Two relevant examples directly linking disruption in protein synthesis and ASD syndromes are Tuberous sclerosis and Fragile-X syndromes, two monogenic form of ASD. Both syndromes are characterized by mutations in a gene encoding for key repressors of the neuronal translation machinery (respectively TSC1/TSC2 and FMRP proteins). Thereby, dysregulation of translational repression leads to major imbalances in protein production, which can result in several neuronal dysfunctions, including over-proliferation, cell death or synaptic dysfunction (Bassell and Warren, 2008; Ehninger and Silva, 2011).

Finally, neuro-inflammation has also been recently linked to the pathophysiology of autism. Human post-mortem brain studies reported microglial activation and astrocytosis in

multiple brain regions, mainly dorsolateral prefrontal cortex and cerebellum (Vargas et al., 2005; Morgan et al., 2010). Additionally, studies found several inflammatory biomarkers in the serum, plasma, and cerebrospinal fluid of children with ASD (Zimmerman et al., 2005). Neuro-inflammation in ASD is not yet well understood and causal genetic variants have not yet been clearly identified. Thereby the question remains on whether neuro-inflammation is a response to upstream neuronal alterations or rather an independent dysfunction.

As highlighted above, the pathophysiology of autism is very diverse and appears to be a "whole body" disorder rather than a single psychiatric condition. Even though converging biological mechanisms have been implicated, no unique biological dysfunction leading to ASD has been identified so far. Current findings support that distinct pathologies converge to a spectrum of cognitive and behavioral disorders defined as ASD. This heterogeneity in the pathophysiology of ASD also makes challenging the identification of predictive biomarkers for early detection. Eye tracking studies show promising results but there is still controversy on whether they constitutes a good predictive ASD biomarker (Pantelis and Kennedy, 2017). Despite the lack of accurate biomarkers, a number of predictive environmental and genetic risk factors have already been identified.

1.2.4 Risk factors

1.2.4.1 Environmental risk factors

Environmental risk factors refer to all factors that are not determined by intrinsic biological mechanisms. Thereby, the term can be interpreted rather widely and englobe mother's drug use, medication, infections, diet, exposure to environmental chemicals or even stress. The embryonic development seems particularly sensitive its surrounding environment but the post-natal period and even parental life style before conception are thought to influence brain development (Lyall et al., 2017). However, demonstrating a clear causal link between an environmental factor and a disorder is often very challenging. Ideally, it would require testing the effect of a single risk factor by keeping all the other parameters unchanged in a representative population sample. This laboratory experimental design is realistically not applicable for overlapping environmental factors acting at different time on individuals with

different ages, life-styles and genetic backgrounds. Most of the recently established environmental risk factors were identified with epidemiological or mouse model studies that provide mainly correlations between a risk factor and ASD. As manifestations develop very early after birth, the time window for environmental factor to contribute to the disorder postnatally is limited. Studies suggest that risk factors are mostly susceptible to act prenatally during embryonic development (Bilder et al., 2009; Buchmayer et al., 2009). The embryonic development is subject to different vulnerability windows but the first trimester of pregnancy appears to be the most sensitive period (Bilder et al., 2009; Buchmayer et al., 2009). The list of environmental triggers is constantly increasing but correlational links are often questionable due to the limited sample size of epidemiological studies and the lack of reproducibility. The following sections highlights only factors with the strongest associative evidence.

Exposure to pharmacological agent during pregnancy is thought to be a major risk factor contributing to neurodevelopmental disorders. Valproic acid, an antiepileptic and mood stabilizer drug, when taken during pregnancy, is well documented to be one of the highest ASD risk factor (Hiilesmaa et al., 1980; Ornoy, 2009; Roullet et al., 2013; Choi et al., 2016). Similarly, Thalidomide another teratogen (banned from sale since the 1960s) is also strongly associated with ASD (Stromland et al., 1994; Rodier, 2002). Misoprostol a prostaglandin analog (prescribed in the treatment of gastric ulcer) and Beta-2 adrenergic drugs (such as terbutaline used in the treatment of asthma) have also been reported to be associated with ASD (Bandim et al., 2003; Witter et al., 2009).

Some virus infection have also been reported to be a high risk factor for autism. Congenital rubella infection appears to be a major risk to develop ASD and, with only moderate evidence, congenital influenza seems to be linked with ASD as well (Libbey et al., 2005). Vaccination gained increasing attention in the early 2000s as being a potential ASD trigger. This resulted largely from a single study, later retracted for a number of scientific inconsistencies including uncontrolled design, small sample size (n=12), and speculative conclusions (Rao and Andrade, 2011). In addition, a number of concerned parents reported that their child developed ASD following vaccinations, without taking in consideration that first signs of ASD arise around the same period than child vaccinations and correlation does

not mean causality. Following these concerns a number of epidemiologic studies have been conducted and consistently showed no link between ASD and vaccines (Hurley et al., 2010; Maglione et al., 2014).

Embryogenesis is particularly sensitive to the mother's environment. Environmental chemicals (mercury, neurotoxicant, pesticides), drug use (cocaine, alcohol), diet (vitamin D deficiency), air pollution and stress exposure during pregnancy are all reported to be potential risk factors for ASD (Lyall et al., 2017). Also, combining these different exposures is very likely to increase probabilities to develop ASD (Lyall et al., 2017).

Recently, the environment of both parents before conception has been suggested to influence the development of the future embryo and lead to ASD phenotypes. Among other factors parental age, stress and life style can influence future embryonic development (Franklin et al., 2010). The current hypothesis suggests that environmental factors can induce epigenetic changes by altering parental genomic activity (changes in methylation of promoter regions) which can be transmitted across generations (Franklin et al., 2010; Saavedra-Rodriguez and Feig, 2013).

Several studies demonstrated that DNA methylation can change in response to environmental factors (Argos, 2015; Joubert et al., 2016) and epigenetic modifications can be inherited (Skinner, 2011). These findings highlight the importance to investigate further the epigenetic and genetic aspect of ASD. To date, it remains unclear what is the exact contribution of environmental versus genetic factors in ASD and to what extend gene-environment interactions weight in the balance of developing the disorder. However, with the constant improvement of sequencing and genome wide association studies, considerable progress has been made in the field.

1.2.4.2 Genetic risk factors

In the late 1970s family and twin studies started to show the high heritability of ASD (Folstein and Rutter, 1977a; Ronald and Hoekstra, 2011). Today, ASD concordance rates between twins varies significantly across studies but ranges between 40-90% for monozygotic

twins and between 15-35% for dizygotic twins (Ronald and Hoekstra, 2011). In parallel, whole genome sequencing and whole-exome sequencing methods further identified a number of rare highly penetrant mutations leading to ASD (Geschwind and State, 2015). These studies clearly highlight the strong genetic contribution to the pathophysiology of ASD.

Mutations can be either inherited or in rare cases arise “de novo” in the germline. ASD inheritance can occur in different ways : *Autosomal recessive*, both healthy parents carry one allele with a recessive mutation; *Autosomal dominant*, one parent carries a dominant mutation; *X-linked*, the mother carries the mutation on the X chromosome (higher risk for males to develop ASD); *Additive mutations*, addition of common genetic variations from both parents.

Genetic mutations can arise in different ways, with a single nucleotide change up to an entire locus. Structural variation of genomic sections, also called copy-number variants (CNV) can be either deleted, duplicated or translocated. Alterations at the nucleotide level can create missense, frameshift, nonsense or trinucleotide repeat mutations. Gene expression can be altered either directly in the exonic and splice site regions creating a truncated protein or indirectly by affecting intronic regulatory regions.

A good illustration of the genetic contribution to ASD, are rare *de novo* mutations; because they appear only in the germline of affected individuals and are not present in the parental genome. Monogenic syndromic forms of ASD usually show high penetrance (frequency with which a particular gene is associated with a given phenotype), ranging between 30-80%. One of the most highly penetrant gene (~80%) is the SHANK3 gene encoding for a synaptic scaffolding protein (Leblond et al., 2014).

Even though single genetic mutations can be highly penetrant, they are found only in a small fraction of ASD population. Each risk gene is present in less than 1% of the affected individuals (see Figure 2). Rare *de novo* and inherited mutations only account each for ~3% of total screened individuals with ASD. Recently it has been suggested that most genetic risks seem to arise from common genetic variation; genomic regions commonly vary across individuals, including mostly polymorphism in single nucleotides (SNP). SNPs are common

base pair changes found in more than 1% of the population. These common variations have been recently proposed to potentially contribute to nearly 50% of ASD cases (Gaugler et al., 2014). Thus, it has been hypothesized that polygenic variations might be the major risk for developing ASD. In other words, inherited variants each contributing to a small fraction, could together produce an additive risk for developing ASD.

Therefore, identifying genetic risk factors is an essential step to further shape the genetic architecture of ASD. In the past years, major advances made in genome sequencing studies allowed the identifications of hundreds of new genes associated with ASD (www.sfari.org/resource/sfari-gene). Currently, advances in the field estimate the genetic etiology of ASD around 30%-50% (de la Torre-Ubieta et al., 2016). For the remaining percentage, it remains to be addressed if the environment, epigenetics, genetics or likely a combination of all will complete the puzzle.

The following Figure adapted from de la Torre-Ubieta et al. (2016) summarizes the genetic aspects of ASD discussed in this section:

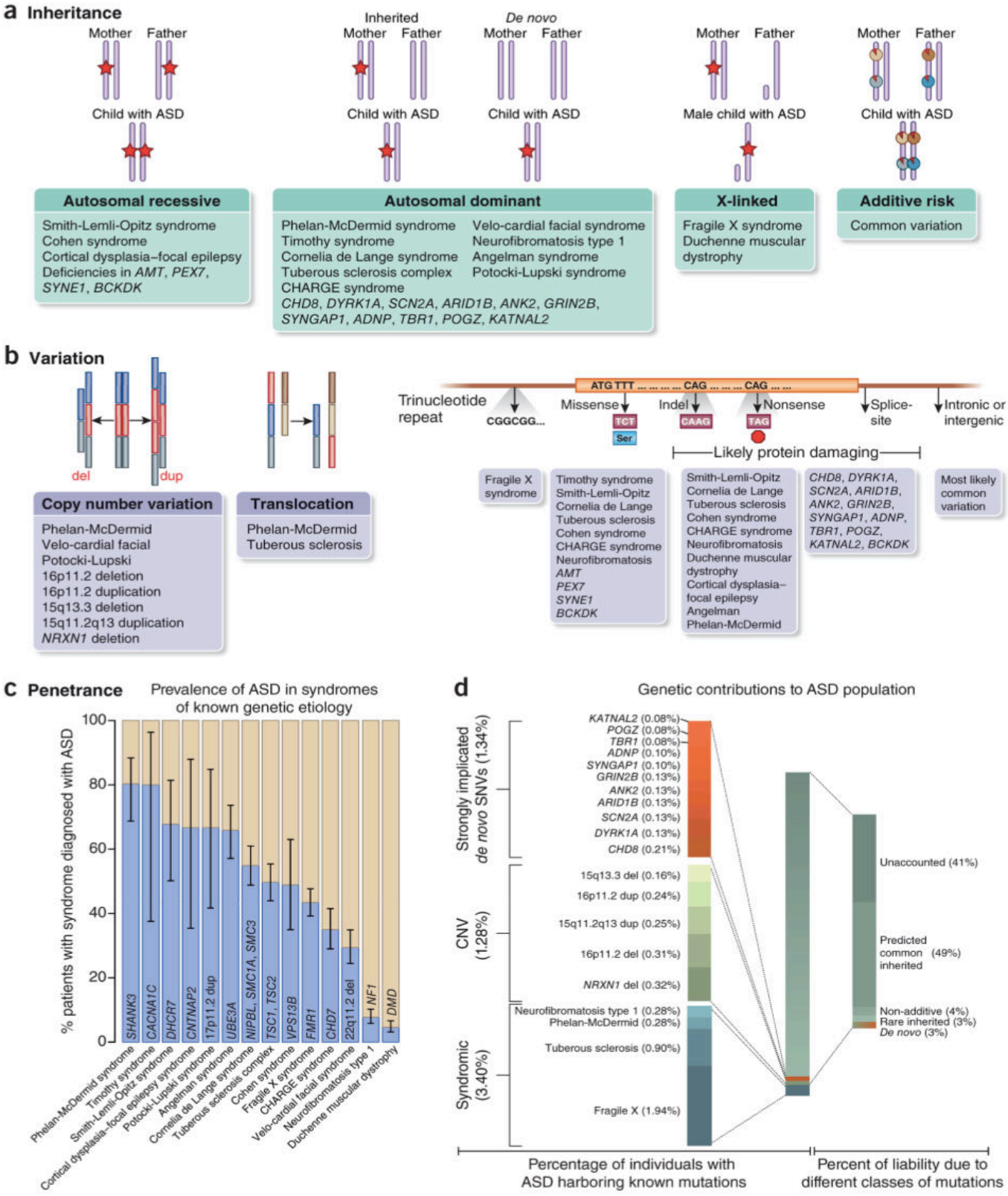
a Inheritance
Mother Father
Child with ASD
Autosomal recessive
Smith-Lemli-Opitz syndrome
Cohen syndrome
Cortical dysplasia–focal epilepsy
Deficiencies in AMT, PEX7, SYNE1, BCKDK
Inherited
Mother Father
Child with ASD
De novo
Mother Father
Child with ASD
Autosomal dominant
Phelan-McDermid syndrome
Timothy syndrome
Cornelia de Lange syndrome
Tuberous sclerosis complex
CHARGE syndrome
CHD8, DYRK1A, SCN2A, ARID1B, ANK2, GRIN2B, SYNGAP1, ADNP, TBR1, POGZ, KATNAL2
Velo-cardial facial syndrome
Neurofibromatosis type 1
Angelman syndrome
Potocki-Lupski syndrome
Mother Father
Male child with ASD
X-linked
Fragile X syndrome
Duchenne muscular dystrophy
Mother Father
Child with ASD
Additive risk
Common variation
b Variation
del
dup
Copy number variation
Phelan-McDermid
Velo-cardial facial
Potocki-Lupski
16p11.2 deletion
16p11.2 duplication
15q13.3 deletion
15q11.2q13 duplication
NRXN1 deletion
Translocation
Phelan-McDermid
Tuberous sclerosis
Trinucleotide repeat
CGGCGG...
ATG TTT ... CAG ... CAG ...
Missense
TCT
Ser
Indel
CAAG
Nonsense
TAG
Splice-site
Intronic or intergenic
Likely protein damaging
Fragile X syndrome
Timothy syndrome
Smith-Lemli-Opitz
Cornelia de Lange
Tuberous sclerosis
Cohen syndrome
CHARGE syndrome
Neurofibromatosis
AMT
PEX7
SYNE1
BCKDK
Smith-Lemli-Opitz
Cornelia de Lange
Tuberous sclerosis
Cohen syndrome
CHARGE syndrome
Neurofibromatosis
Duchenne muscular dystrophy
Cortical dysplasia–focal epilepsy
Angelman
Phelan-McDermid
CHD8, DYRK1A, SCN2A, ARID1B, ANK2, GRIN2B, SYNGAP1, ADNP, TBR1, POGZ, KATNAL2, BCKDK
Most likely common variation
c Penetrance
Prevalence of ASD in syndromes of known genetic etiology
% patients with syndrome diagnosed with ASD
100
80
60
40
20
0
SHANK3
CACNA1C
DHCR7
CNTNAP2
17p11.2 dup
UBE3A
NIPBL, SMC1A, SMC3
TSC1, TSC2
VPS13B
FMR1
CHD7
22q11.2 del
NF1
DMD
Phelan-McDermid syndrome
Timothy syndrome
Smith-Lemli-Opitz syndrome
Cortical dysplasia-focal epilepsy syndrome
Potocki-Lupski syndrome
Angelman syndrome
Cornelia de Lange syndrome
Tuberous sclerosis complex
Cohen syndrome
Fragile X syndrome
CHARGE syndrome
Velo-cardial facial syndrome
Neurofibromatosis type 1
Duchenne muscular dystrophy
d
Genetic contributions to ASD population
Strongly implicated de novo SNVs (1.34%)
KATNAL2 (0.08%)
POGZ (0.08%)
TBR1 (0.08%)
ADNP (0.10%)
SYNGAP1 (0.10%)
GRIN2B (0.13%)
ANK2 (0.13%)
ARID1B (0.13%)
SCN2A (0.13%)
DYRK1A (0.13%)
CHD8 (0.21%)
CNV (1.28%)
15q13.3 del (0.16%)
16p11.2 dup (0.24%)
15q11.2q13 dup (0.25%)
16p11.2 del (0.31%)
NRXN1 del (0.32%)
Syndromic (3.40%)
Neurofibromatosis type 1 (0.28%)
Phelan-McDermid (0.28%)
Tuberous sclerosis (0.90%)
Fragile X (1.94%)
Unaccounted (41%)
Predicted common (49%) inherited
Non-additive (4%)
Rare inherited (3%)
De novo (3%)
Percentage of individuals with ASD harboring known mutations
Percent of liability due to different classes of mutations

Figure 2. Genetic architecture of ASD (de la Torre-Ubieta et al., 2016). (a) Different inheritance pattern and their associated syndromic form of ASD. The red stars indicate a causal allele and the red pie charts indicate a small proportion of risk. (b) The types of genetic variations and the associated developmental disorders. (c) The penetrance of known syndromic mutations summarized from multiple studies. 95% binomial proportion confidence intervals, based on Wilson's score interval. (d) The percentage of individuals with ASD harboring known mutations, as well as the percentage of liability from different classes of mutations. The percentage variance in liability measures the contribution of a particular variant or class of variants relative to the population variance in a theoretical variable called liability. Liability is a continuous and normally distributed latent variable that represents each individual's risk (both genetic and environmental) for developing a disease.

Understanding the pathophysiology of ASD not only requires the identification of risk genes but also the study of their biological function. As described in section **1.2.3** a number of converging biological pathways have already been identified, however targeted molecular therapies can be considered only if convergent pathways are better defined.

1.2.5 The importance of model systems

Human brain surveys offer a limited number of biological information. Patient studies can only provide behavioral, metabolic and brain network information. Post-mortem tissues availability is generally limited and tissues are often genetically very heterogeneous. Thereby, system models are necessary to rigorously study the biological implications of risk genes. Mouse models are the main biological system used so far. The mouse genome can be targeted with genetic engineering tools to specifically alter a gene of interest and study the downstream effects. Mouse models offers a number of advantages: they share high genomic homology with humans, they reproduce fast with large litters, are cost-effective, offer reproducibility, genetic traceability and most importantly accessibility to molecular, cellular, circuit and behavioral experimentations. However, mice models also have some limitations. The evolutionary distance involves a number of biological differences, including poorly conserved regulatory elements, differences in the social circuitry and limitations in behavioral read-outs.

Alternatively to mice models, human cells can be used to study ASD. Advances in stem cell biology made possible to culture human embryonic stem cells, human induced pluripotent stem cells (iPSCs) and primary human neural progenitors (Aigner et al., 2014). To model ASD, cells can either be cultured directly from patients (from surgery or post-mortem) or genetically targeted (with genetic engineering tools such as the CrispR-Cas9 system). Recently, a major advance in the field made possible long-term three-dimensional culture of iPSCs, giving rise to organoid brain like structures (Lancaster et al., 2013). This way, iPSCs can be isolated from ASD patient that underwent brain surgery (tissue removed from epileptogenic regions) and provide a good model system. Alternatively, targeted mutations can be induced as well in organoid cultures to model ASD (Pasca, 2018).

Mice, and more recently human *in vitro* models, provided most of the current knowledge regarding the biological understanding of ASD. Using model systems to study individual risk genes not only provides essential information on their function but also further shapes the complex pathophysiology of ASD.

1.3 PTCHD1: a poorly understood risk gene for ASD

1.3.1 Human PTCHD1 mutations are linked with ASD and ID

In 2008, a genome-wide study comparing CNVs of 427 unrelated ASD patients to 500 unaffected individuals, identified the Patched domain containing 1 (PTCHD1) locus as a risk factor for ASD (Marshall et al., 2008). Later, Pinto et al. (2010) confirmed this finding in a larger scale sequencing studies comparing 996 ASD cases to 1287 unaffected controls. Identified mutations were all CNV deletions inherited from mothers X chromosome. Similarly, Whibley et al. (2010) conducted a fine scale study focusing specifically on X chromosome linked intellectual disability (XLID). 251 cases diagnosed with XLID were analyzed with an X chromosome array platform. A 90 kb deletion spanning the entire PTCHD1 gene was identified in a family with XLID affected males across two generations (mutated allele carried by the unaffected grandmother). Subsequently, Noor et al. (2010) focused specifically on validating and characterizing the PTCHD1 CNVs and their inheritance in the families. They conducted a large scale meta-analysis on three ASD data sets (total: ASD N=1843, ID N=246, ADHD N=167, controls N=10896). The study validated with real-time quantitative PCR (RT-qPCR) the heritability of previously identified CNV deletions from Marshall et al., Pinto et al. and Whibley et al. Further, for 10 ASD cases deletions were mapped upstream of PTCHD1 coding region. This suggests a potential involvement of upstream regulatory element in PTCHD1 linked disorders. Finally six cases of point mutations in unrelated ASD families and two ID families were found, suggesting that truncations in the Ptchd1 protein are sufficient to trigger ASD or ASD like phenotypes. Findings from Noor et al. suggest that PTCHD1 mutations occur in ~1% of ASD cases, however this estimation has not been confirmed yet. Taken together these sequencing surveys indicate that PTCHD1 is a highly inheritable and penetrant risk gene strongly associated with ASD and ID.

A clinical study by Chaudhry et al. (2015) documented the phenotypic alterations on 23 PTCHD1 mutated individuals. All affected cases were males except one female. Clinical assessments were done at different ages but 18 out of 23 patients were evaluated before age 13. As summarized in Figure 3, around 40-45% of them displayed either core or associated ASD symptoms, with a certain degree of overlap between conditions. In addition, several of them had motor delays and half of them displayed a hypotonic face, suggesting a potential involvement of PTCHD1 in muscular function.

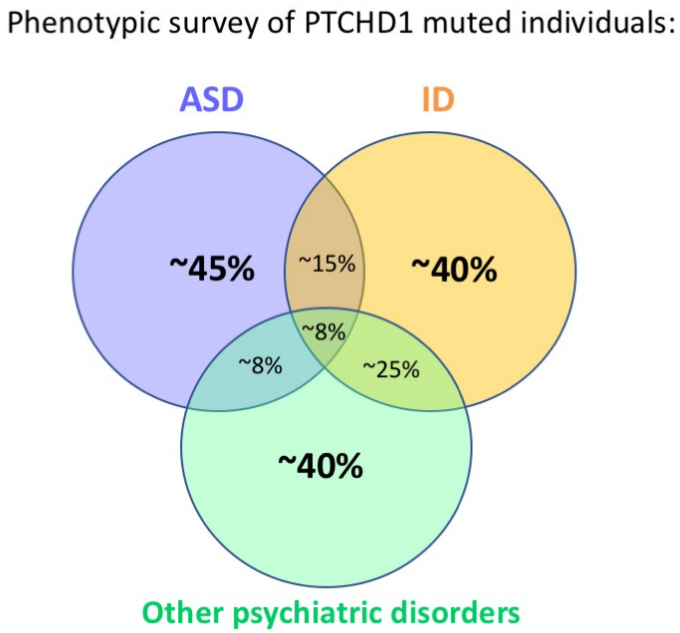

Figure 3. Prevalence of core and associated ASD symptoms in PTCHD1 muted individuals. Estimations were calculated from Chaudhry et al. (2015) on N=23 individuals. "Other psychiatric disorders" shown in green include anxiety, aggression, attention deficit, hyperactivity, depression.

Overall, this survey suggests that all 23 individuals carrying PTCHD1 mutations were affected by either a neurodevelopmental, a cognitive and/or a psychiatric disorder. However, a larger study would be needed to confirm whether these estimations on 23 cases are representative. The main obstacles to perform such large-scale studies is finding patients

carrying the mutation of interest. Even if PTCHD1 mutations appear to occur at higher rate than most of the risk genes, they remain rare in the overall ASD population.

Documenting the phenotypic outcomes of a single gene mutation is an essential step to link a gene with a pathology. However, this does not provide any information on how a gene mutation leads to downstream dysfunctions. This requires neurobiologists to focus on the gene product and its implications at a molecular, cellular, circuit and behavioral level.

1.3.2 The PTCHD1 gene is predicted to produce a transmembrane protein

The PTCHD1 gene is located on the X chromosome, composed by 13714 base pair with three exonic regions. It encodes for a 888 amino acid protein predicted to form a twelve pass transmembrane protein, as shown in Figure 4.

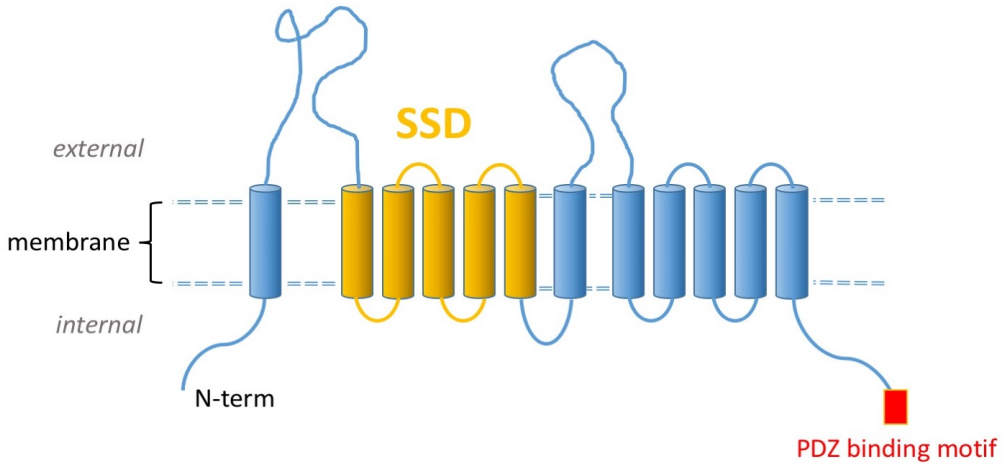

Figure 4. Schematic representation of the Ptchd1 protein. The twelve pass transmembrane protein carries a sterol sensing domain (SSD, shown in yellow) and a PDZ binding motif (shown in red) at the C-terminal of the protein.

As shown on Figure 4, Ptchd1 carries a sterol sensing domain (SSD) capable of binding sterols. In addition, the protein possesses a PDZ binding motif, a short C-terminal amino-acid motif that binds proteins carrying a PDZ domain. Proteins with PDZ domains are involved in scaffolding, transporting and organizing signaling complexes at the membrane, especially at

the synapse. These two components (SSD and PDZ binding motif) will be subject of different hypotheses and discussion later in this manuscript.

As shown on Figure 5, PTCHD1 appeared early in eukaryotic evolution and displays very few changes within mammalians with around 95% average sequence identity (calculated with Uniprot alignment tool). Such high genetic conservation can suggest its implication in essential biological processes necessary for the survival of an organism.

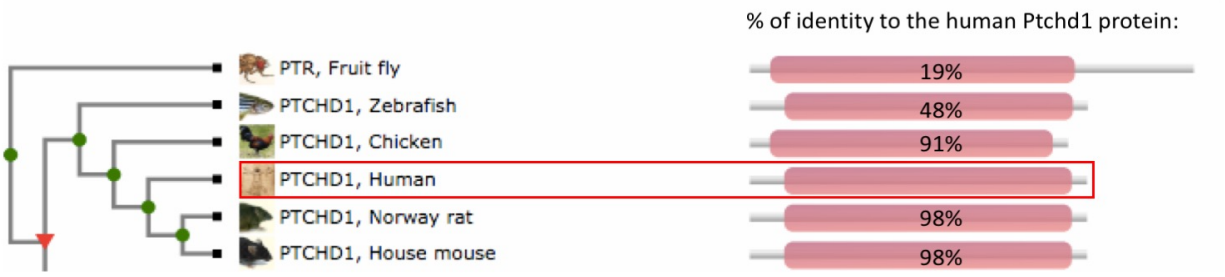

Figure 5. Gene tree of PTCHD1. (Modified from www.treefam.org). Left, Evolutionary genetic distances of PTCHD1 across species. Right, Percentage of amino acid identity to the human Ptchd1 protein.

PTCHD1 is the member of a family of three other "patched domain like" proteins: PTCHD2, 3 and 4. Compared to PTCHD1, these three proteins have very low or no expression in the brain (allenbrain data) and they have not been link with any neurodevelopmental disorder or disease. Moreover, a sequencing study showed no association between individuals with PTCHD3 mutations and ASD (Ghahramani Seno et al., 2011).

1.3.3 Ptchd1 is hypothesized to be a Sonic hedgehog receptor

The four "patched domain like" proteins carry this nomenclature because they share a SSD with the well characterized patched (Ptch) protein (Kuwabara and Labouesse, 2002). As shown in Figure 6, the SSD is highly conserved in six families of proteins:

(1) hydroxymethylglutaryl-CoA reductases (HMDHs), cholesterol biosynthetic enzymes degraded when sterol levels are high;

(Andersen and Koeppe) SREBP (sterol regulatory element binding protein) cleavage activating proteins (SCAPs),

(3) Niemann-Pick C-1 type protein (NPC1), an intracellular cholesterol transporter;

(4) Dispatched proteins, involved in releasing the cholesterol-bound hedgehog;

(5) Patched proteins, receptors of the morphogen factor sonic hedgehog (Shh);

(6) Patched-related (or patched domain like) proteins.

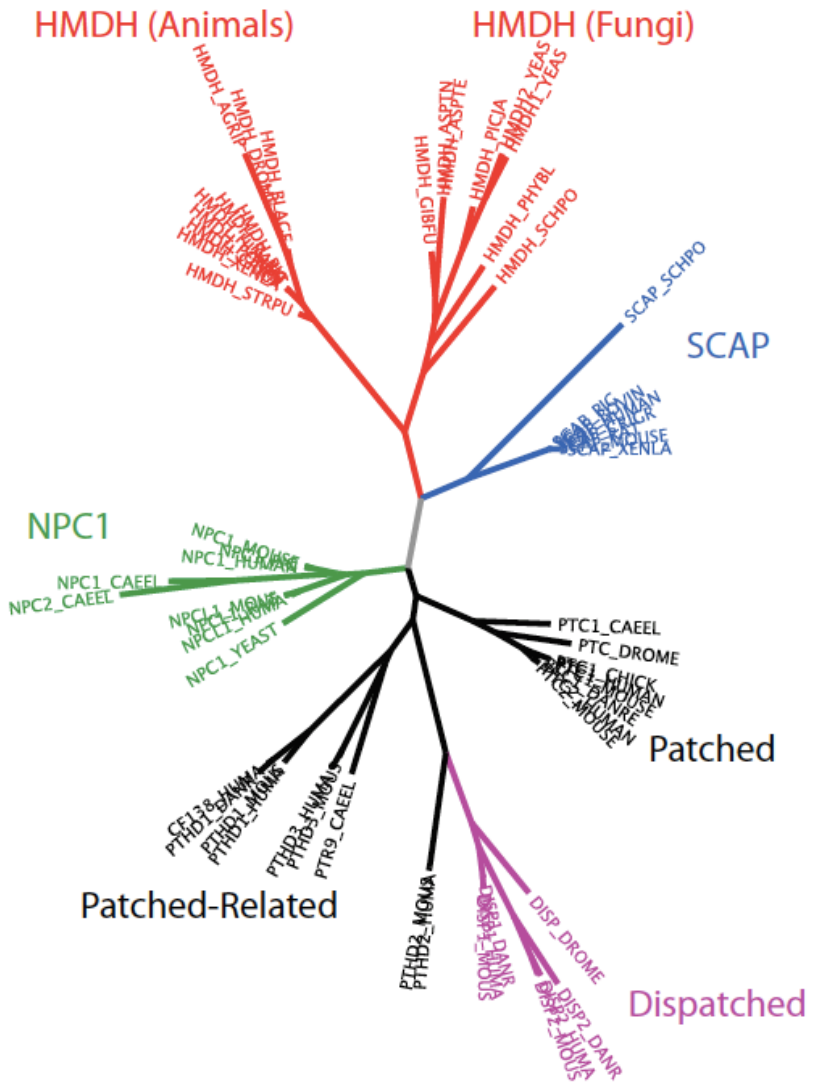

Figure 6. Phylogenetic tree of sterol sensing domains. Adapted from Strope et al. (2009). The maximum likelihood phylogenetic tree of 59 SSD regions. Six families of proteins clearly cluster separately. The Patched-related family cluster closely to the NPC1 and Patched family. The MAFFT tool was used for multiple alignment and the RAXML tool was used to reconstruct the phylogenetic tree.

As shown in Figure 6, Ptchd1 shares a highly conserved SSD primarily with the morphogen receptor Ptch and the cholesterol transporter NPC1. Shh, the ligand of Ptch, carries a sterol group that binds onto the SSD of Ptch and induces the inactivation of the transcription repressor Smoothend (Smo). Smo represses the activity of the GLI transcription factors. Thereby the binding of Shh onto Ptch will indirectly activate a number of GLI dependent transcriptional processes essential for correct morphogenesis and neuronal proliferation.

Based on this well characterized pathway and sequence similarities, Noor et al. (2010) assessed if Ptchd1 could have a similar function than Ptch and thereby performed an *in vitro* GLI dependent reporter assay. The activity of a luciferase reporter dependent on GLI was measured in cells over expressing either Ptch1,2 or Ptchd1. Despite a number methodological inconsistency, the study concluded that similarly to Ptch1 and 2, Ptchd1 represses GLI dependent transcription *in vitro*. Based on this transcriptional reporter assay and the conserved SSD, it was hypothesized that Ptchd1 may contribute to Shh signaling (Noor et al., 2010). Until the beginning of my PhD project in 2014, this hypothesis had not been further investigated and the exact molecular function of Ptchd1 stayed unclear.

Note: *Towards the completion of my PhD, two other studies contributed to the characterization of Ptchd1 (Wells et al., 2016; Ung et al., 2017). As this manuscript follows a chronological order to justify the aims of the project, the contribution of the two studies will be treated in the discussion part (section 3.)*

1.4 The dissertation project

As introduced, dissecting the etiology of ASD by characterizing the function of risk genes is essential to identify convergent pathways and thereby find targeted molecular therapies. PTCHD1 is a highly penetrant and prevalent gene found in individuals with ASD and ID (Noor et al., 2010; Chaudhry et al., 2015). The gene produces a twelve-pass transmembrane protein that shares a SSD domain with Ptch and NPC1 (Kuwabara and Labouesse, 2002; Noor et al., 2010). As described earlier, Ptchd1 was hypothesized to contribute to Shh signaling (Noor et al., 2010). In addition, a number of studies showed that alterations in the Pch-Shh pathway lead to severe deficits; Heterozygous or conditional homozygous mutations of Ptch result in Shh-independent activation of the signaling molecule Smoothened. Hyper-activation of Smoothened regulation results in neuronal precursor over-proliferation, enlargement of the external germinal layer of the cerebellum, and the development of medulloblastomas (Goodrich et al., 1997; Yang et al., 2008). Recent studies have identified Boc and Gas1 as obligate co-receptors for Shh signaling in the cerebellum. Their loss of function results in reduced Shh-dependent proliferation of precursors (Izzi et al., 2011) and cerebellar abnormalities. Given these well-documented functions of the Shh-Ptch1 pathway, we generated a knock-out mouse model to start examining whether neuronal precursor proliferation was altered in Ptchd1 knock-out (*Ptchd1*$^{-/y}$) mice. This first hypothesis was embedded in a broader question asking what is the molecular and cellular function of Ptchd1 in the brain. This question was the main driver of my project and set the following milestones:

(1) Localize PTCHD1 expression in the brain at an anatomical and cellular level
(2) Assess Ptchd1 involvement in the Shh pathway using a *Ptchd1*$^{-/y}$ mouse model
(3) Identify Ptchd1 interacting partners
(4) Characterize Ptchd1 function *in vitro* and *in vivo* with the loss of function model

2. Results

Note: *The following results were published in the Journal of Neuroscience in November 2017: (Tora et al., 2017), except for section "2.7 Preliminary result". The electrophysiological recording were done by Dr. Andrea Gomez and the in vitro Shh binding assay was done by Patricia T. Yam and Jean-Francois Michaud from the laboratory of Pr. Frédéric Charron. The text used in the result section is adapted from the publication, except for section 2.7, which is new unpublished data.*

2.1 Developmental regulation of Ptchd1 expression in the mouse brain

To identify cell populations in the mouse brain with high *Ptchd1* expression we used in situ hybridization with a probe directed against the 5' UTR (exon 1) of mouse *Ptchd1*. In developing mouse brain (postnatal day 12), we observed significant hybridization signals across the entire brain with high signals in the thalamic reticular nucleus and the cerebellum. In the cerebellum, there was significant expression in the external germinal layer, a site where granule cell precursors proliferate before they initiate their migration towards the internal granular layer (Figure 7A). In adult mice (postnatal day 60) we found highest hybridization signals in the internal granular layer of the cerebellum, the reticular nucleus of the thalamus, and in the dentate gyrus of the hippocampus, consistent with a previous report (Wells et al., 2016) (Figure 7B).

Previous work reported synaptic deficits in the hippocampus of Ptchd1 mutant mice (Ung et al., 2017). Thus, we sought to obtain additional, more quantitative insights into *Ptchd1* expression in this brain area. Fluorescent in situ hybridization with *Ptchd1*-specific probes revealed high *Ptchd1* mRNA expression in dentate granule cells of 21 day old mice whereas expression in the CA1-3 pyramidal cells was very low (Figure 7C,E,F). Similarly, high hybridization signals were observed in the dentate gyrus of adult (P60) mice (Figure 7D).

Quantitative PCR measurements for *Ptchd1* mRNA across multiple brain areas confirmed broad expression and developmental regulation of the *Ptchd1* transcript (Figure 7G). In the cerebellum, there was a 2-3 fold up-regulation of Ptchd1 relative to *Gapdh* from

postnatal day 15-30 (Figure 7G, a similar up-regulation was observed when *Hprt* was used as a normalizer).

To further confirm differential expression of Ptchd1 mRNA across the principal cell types of the hippocampal circuit we micro-dissected dentate gyrus and Ammon's Horn from P21 mice and performed quantitative PCR analyses (Figure 7H). Again, we observed high expression of Ptchd1 mRNA in dentate gyrus and low expression in Ammon's horn preparations. Together, these observations support significant expression of *Ptchd1* mRNAs in the developing and adult brain, and particularly prominent expression in the thalamic reticular nucleus, hippocampal dentate granule cells, and cerebellar granule neurons.

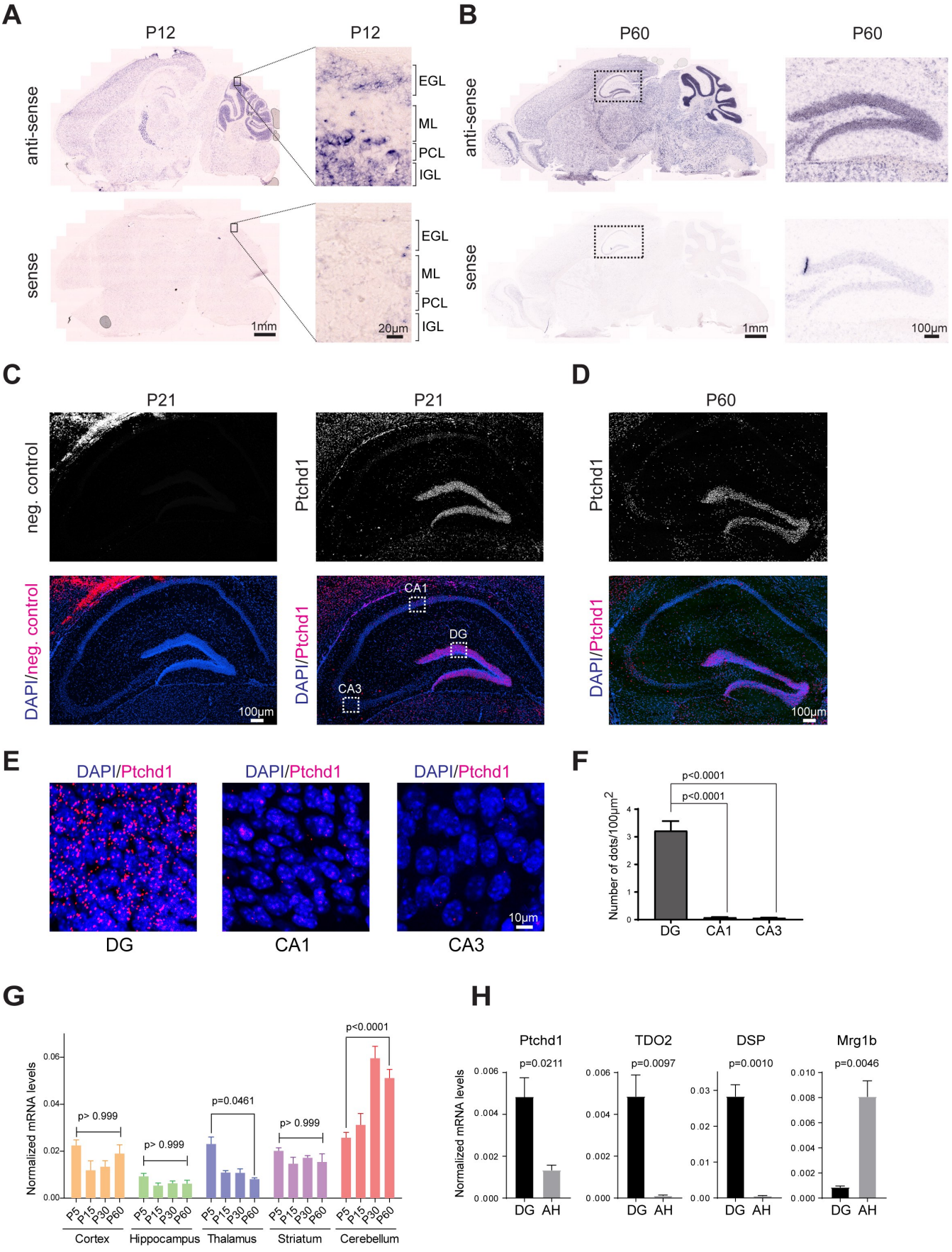
A
P12
P12
anti-sense
sense
EGL
ML
PCL
IGL
1mm
20μm
B
P60
P60
anti-sense
sense
1mm
100μm
C
P21
P21
neg. control
Ptchd1
DAPI/neg. control
DAPI/Ptchd1
CA1
DG
CA3
100μm
D
P60
Ptchd1
DAPI/Ptchd1
100μm
E
DAPI/Ptchd1
DAPI/Ptchd1
DAPI/Ptchd1
10μm
DG
CA1
CA3
F
p<0.0001
p<0.0001
Number of dots/100μm2
DG
CA1
CA3
G
Normalized mRNA levels
p> 0.999
p> 0.999
p=0.0461
p> 0.999
p<0.0001
P5
P15
P30
P60
Cortex
Hippocampus
Thalamus
Striatum
Cerebellum
H
Ptchd1
TDO2
DSP
Mrg1b
p=0.0211
p=0.0097
p=0.0010
p=0.0046
Normalized mRNA levels
DG
AH

Figure 7. *Ptchd1* mRNA distribution in the mouse brain. A, *Ptchd1 in situ* hybridization on mouse brain sagittal sections at post-natal day 12 (P12) with antisense (up) and sense probes (down). High magnification view of the developing cerebellum (right; EGL: external granule cell layer; ML: molecular layer; PCL: Purkinje cell layer; IGL: Internal cell layer). B, *Ptchd1 in situ* hybridization at P60 with with antisense (up) and sense probes (down). High magnification view of the dentate gyrus (Yang et al.). C, Fluorescent in situ hybridization of mouse P21 hippocampus with negative control probe set (left) and Ptchd1 probe set (Yang et al.). DAPI in blue; *Ptchd1* mRNA in magenta. D, Fluorescent in situ hybridization of mouse P60 hippocampus with Ptchd1 probe set; nuclei stained with DAPI in blue; *Ptchd1* mRNA in magenta. E, High magnification view of the dentate gyrus (DG), CA1 and CA3 of the hippocampus (P21 WT mouse coronal section). F, Quantification of fluorescent signal, measured as number of dots in whole DG, CA1 and CA3 area. (N=3 P21 mice, n=22 coronal sections both hemispheres analyzed; mean and SEM; student t-test). G, Quantitative RT-PCR assay of *Ptchd1* mRNA expression levels during brain development and across different brain regions (N=3 mice per age, mean and SEM, one way ANOVA, Tukey's multiple comparisons test). H, Quantitative RT-PCR assay of *Ptchd1* mRNA expression levels in micro-dissected dentate gyrus (DG) and Ammon's horn (AH). TDO2 and DSP serve as control to confirm DG tissue enrichment. Mrg1b serves as control to confirm isolation of Ammon's horn tissue (AH). (N=3 P21 mice, mean and SEM; Student t-test).

2.2 Ptchd1 knock-out mouse generation

To examine essential functions of *Ptchd1* we generated a conditional knock-out allele where exon 2 is flanked by loxP sites (Figure 8A). We then generated a germline *Ptchd1* mutant (*Ptchd1*$^{-/y}$) by crossing with Cre-deleter mice. Using RT-PCR we observed a loss of exon 2 containing sequences and detected transcripts containing exon 1 sequences joined to exon 3 (Figure 8B).

Due to a frame-shift, these transcripts carry a translational stop codon 93 amino acids into exon 3, resulting in the loss of 9 of the 12 transmembrane-domains and disruption of the sterol-sensing domain of the Ptchd1 protein.

To examine the impact of exon 2 deletion on Ptchd1 protein expression we raised polyclonal antibodies and probed Ptchd1 protein levels in Western blots. In transfected HEK293 cells, Ptchd1 antibodies specifically recognized EGFP-tagged Ptchd1 protein of 120 kDa (Figure 8C). In mice, we detected a 95kDa protein in lysates from adult mouse wild-type hippocampus and cerebellum that was absent in male *Ptchd1*$^{-/y}$ mice (Figure 8D). Using the same antibody, we further confirmed broad Ptchd1 protein expression as well as high expression in the mouse cerebellum (Figure 8D).

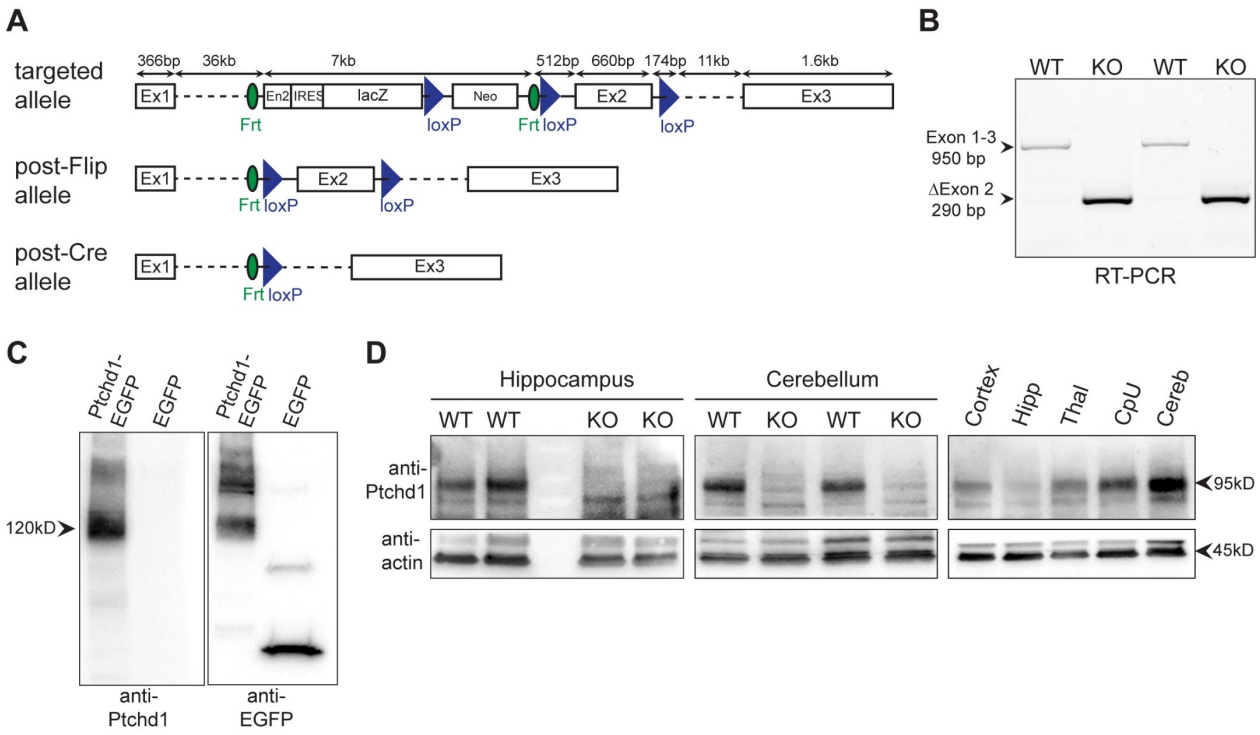

Figure 8. *Ptchd1* knock-out mouse generation and validation. A, *Ptchd1* knock-out strategy, the *Ptchd1* gene was modified by replacing exon 2 with cassette containing a gene trap lacZ-Neo cassette (engrailed 2 splicing acceptor) flanked by Frt sites and additional loxP sites flanking Exon 2. Conditional *Ptchd1* floxed animals were obtained by breeding to Flip deleter mice, resulting in an excision of the trap cassette. The *Ptchd1* knock-out allele was generated by crossing *Ptchd1* floxed animals with CMVcre deleter mice. B, RT-PCR of WT and *Ptchd1*$^{-/y}$ cDNA; shows successful removal of Exon 2 and splicing of exon 1 into exon 3, resulting into a frame-shift. Splice junctions were confirmed by DNA sequencing. C, Specificity of a Ptchd1-specific antibody was confirmed by Western blot analysis of HEK293T cells overexpressing a Ptchd1-EGFP fusion protein. D, Successful ablation of Ptchd1 protein in knock-out animals was verified by Western blot analysis of hippocampal tissue lysate (left) and cerebellar tissue lysate (middle). Right, Ptchd1 protein relative expression levels across brain regions in adult P60 mouse. Similar results were obtained in 3 independent experiments.

2.3 Proliferation of neuronal precursors in Ptchd1$^{-/y}$ mice

Ptchd1 has been suggested to act as a Shh receptor (Noor et al., 2010). During early postnatal development, cerebellar granule cell precursors proliferate in response to Purkinje cell-derived Shh (Wechsler-Reya and Scott, 1999) and homo- or heterozygous knock-out of the Shh receptor Patched 1 (Ptch1) results in granule cell precursor over-proliferation (Goodrich et al., 1997; Yang et al., 2008). Given the high expression of *Ptchd1* in granule cell precursors during early postnatal development we tested whether precursor proliferation was altered in *Ptchd1*$^{-/y}$ mice.

We injected mice at postnatal day 4 (P4, a time where Shh-dependent proliferation is high) with 100mg/kg BrdU and then probed the number of BrdU-positive cells 30 mins after injection. Using this protocol, the density of BrdU-positive cells as well as the density of cells immuno-positive for the proliferation marker phospho-histone 3 (PH3) were unchanged in *Ptchd1*$^{-/y}$ mice (Figure 9A,B).

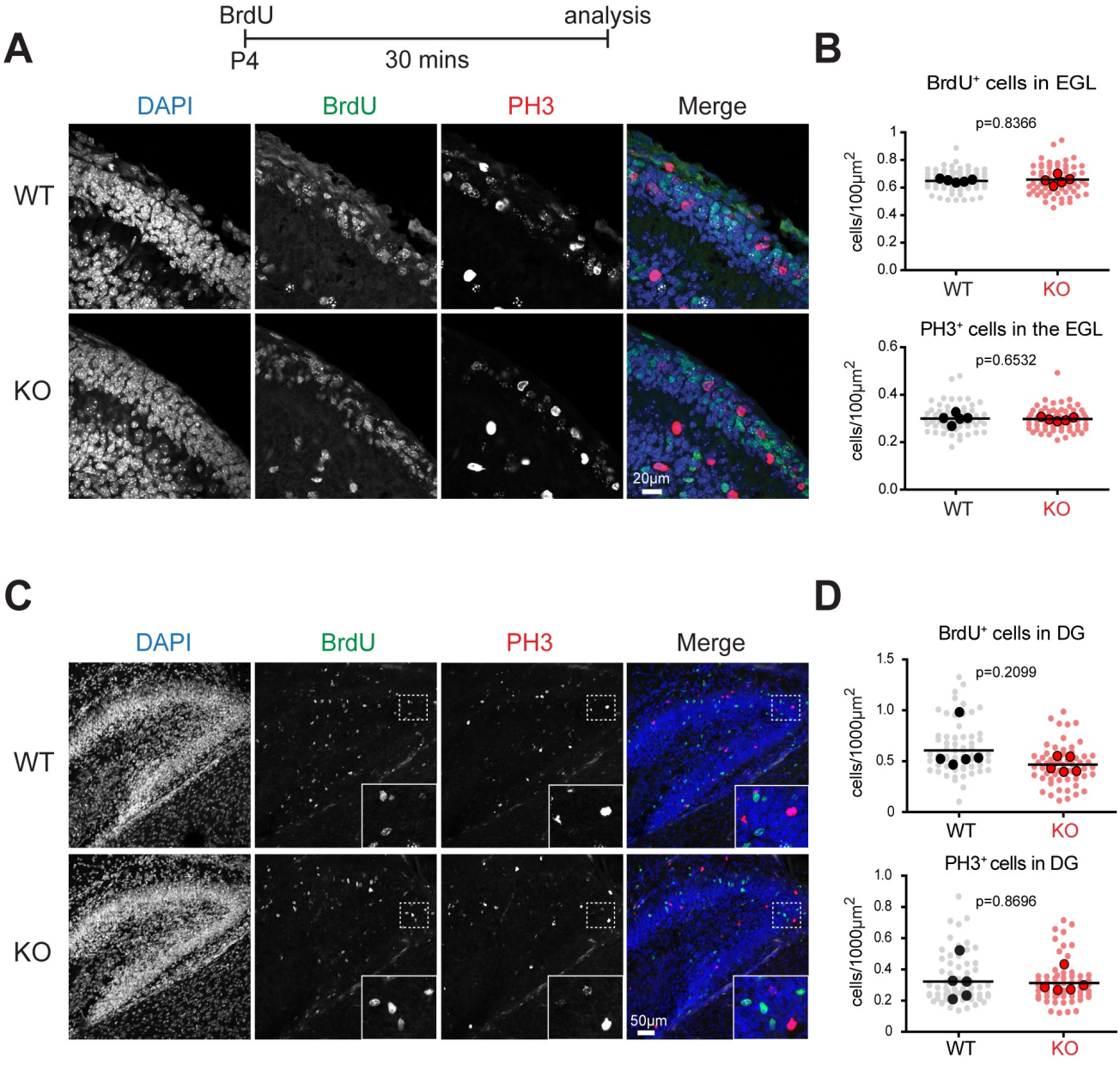

Figure 9. Proliferation of neuronal precursors in developing Ptchd1$^{-/y}$ mice. **A**, Wild-type (WT) and *Ptchd1*$^{-/y}$ (KO) mice were injected with 100mg/kg BrdU at postnatal day 4 (P4) and analyzed 30 mins later. Cerebellar sections were stained for BrdU, PH3 and DAPI. **B**, Quantification of BrdU- and PH3-positive cell density in the EGL. Cell counts are normalized to the EGL area. Mean and standard deviation from N=5 mice per genotype; n= 65 *Ptchd1*$^{-/y}$, 61 WT sections (light dots); solid dots are means of cell density per animal; unpaired t-test. **C**, Hippocampal sections of P4 WT and *Ptchd1*$^{-/y}$ (KO) mice stained for BrdU, DAPI. Insets show enlargements of the area marked with a dashed box. **D**, Quantification of BrdU and PH3-positive cell density in the DG. Cell density was normalized to the DG area. Mean and standard deviation, from N=5 mice per genotype; n= 61 *Ptchd1*$^{-/y}$, 61 WT sections (light dots); solid dots are means of cell density per animal; unpaired t-test.

A second neuronal precursor population that is dependent on Shh signaling during development are granule cells in the dentate gyrus of the hippocampus (Han et al., 2008; Li et al., 2013). Thus, we quantified BrdU- and PH3-positive cells in wild-type and *Ptchd1*$^{-/y}$ mice. Similar, to the cerebellum, BrdU-incorporation and density of PH3-positive cells was not significantly changed (Figure 9C, D). We then tested BrdU incorporation in adult (P60) dentate gyrus since Shh has also been implicated in the maintenance of adult neural stem cells in this area (Lai et al., 2003). However, in *Ptchd1*$^{-/y}$ mice we did not detect a significant change in the density of PH3 or BrdU-positive cells 4 days after BrdU injection (Figure 10A, B).

Our results thus far suggest that the absence of Ptchd1 has no dramatic effect on neuronal precursor proliferation in vivo in cell populations that undergo Shh-dependent proliferation. To directly determine if Ptchd1 may interact with Shh, we tested whether Shh can bind in vitro to cells expressing Ptchd1 protein.

We observed robust binding of Shh to COS7 and mouse embryonic fibroblast (MEF) cells expressing Ptch1 but no binding to cells expressing Ptchd1 nor NPC1 under identical experimental conditions (Figure 10C). Thus, 50% of COS7 cells and 78% of MEFs expressing Ptch1 exhibited clearly recognizable Shh surface binding whereas none of the cells expressing Ptchd1, GFP or NPC1 did (Figure 10D). In aggregate, these experiments suggest that expression of Ptchd1 is not essential for the Shh-dependent proliferation or maintenance of neuronal precursors in the developing cerebellum or the postnatal dentate gyrus.

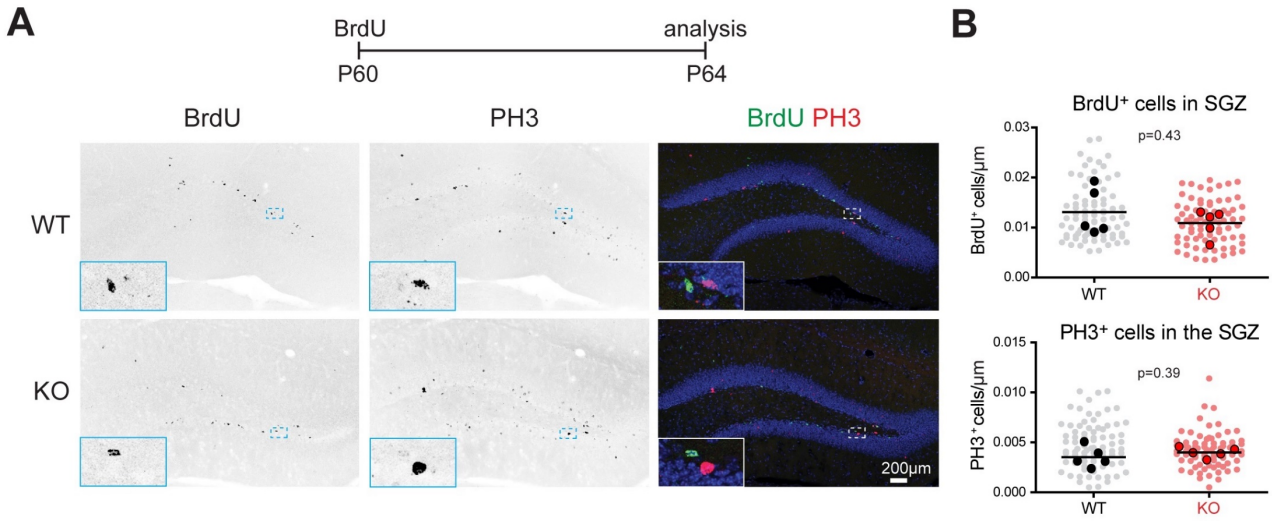
A
BrdU
analysis
P60
P64
BrdU
PH3
BrdU PH3
WT
KO
200μm
B
BrdU⁺ cells in SGZ
p=0.43
BrdU⁺ cells/μm
0.03
0.02
0.01
0.00
WT
KO
PH3⁺ cells in the SGZ
p=0.39
PH3⁺ cells/μm
0.015
0.010
0.005
0.000
WT
KO

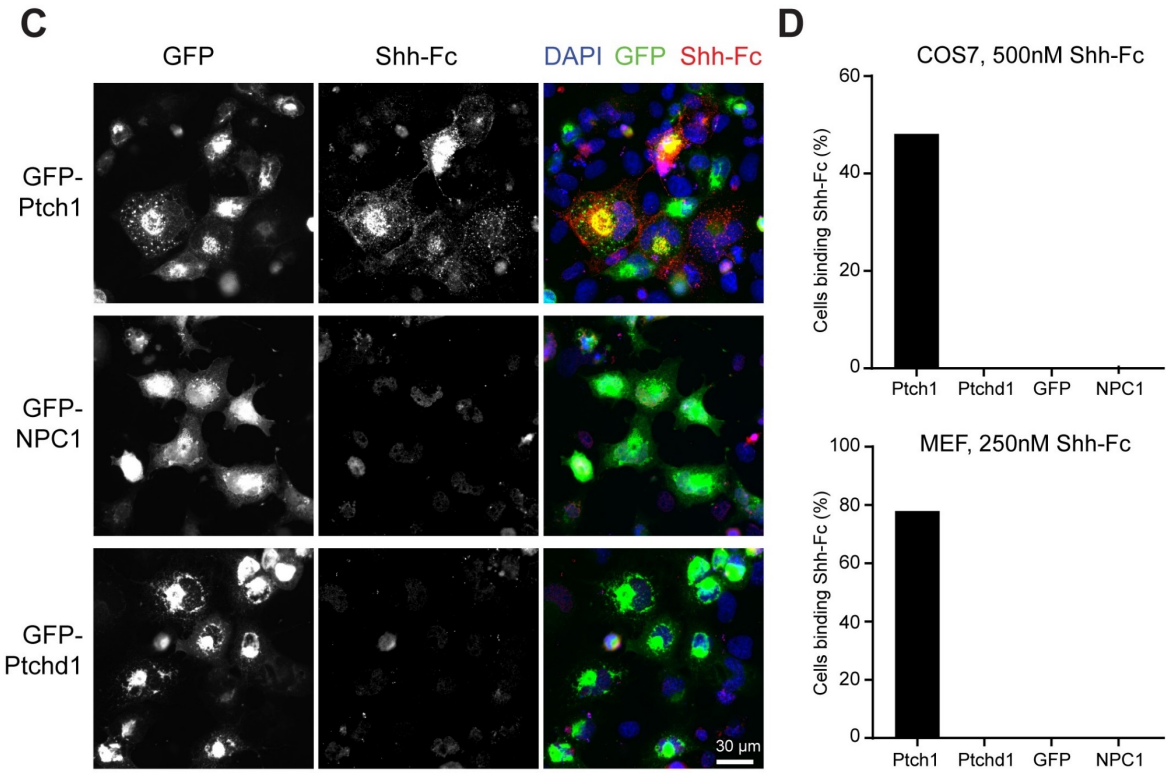
C
GFP
Shh-Fc
DAPI GFP Shh-Fc
GFP-
Ptch1
GFP-
NPC1
GFP-
Ptchd1
30 μm
D
COS7, 500nM Shh-Fc
Cells binding Shh-Fc (%)
60
40
20
0
Ptch1
Ptchd1
GFP
NPC1
MEF, 250nM Shh-Fc
Cells binding Shh-Fc (%)
100
80
60
40
20
0
Ptch1
Ptchd1
GFP
NPC1

Figure 10. Adult neurogenesis in Ptchd1$^{-/y}$ mice and Shh binding to Ptchd1. A, Wild-type (WT) and *Ptchd1*$^{-/y}$ (KO) mice were injected with 100mg/kg BrdU at postnatal day 60 (P60) and analyzed 4 days later (P64). Hippocampal sections of WT and *Ptchd1*$^{-/y}$ (KO) mice were stained for the DAPI (blue), BrdU (Pinto et al.) and PH3 (red). Insets show enlargements of the area marked with a dashed box. B, Quantification of BrdU- and PH3-positive cell density in the sub-granular zone (SGZ) of the dentate gyrus. Cell numbers were normalized to SGZ length. Mean and standard deviation. n=156 *Ptchd1*$^{-/y}$, 160 WT dentate gyrus regions analyzed (light dots) from N=5 mice per genotype (solid dots are means of cell density per animal), unpaired t-test. C, Sonic hedgehog (Shh) binding assay on COS cells over-expressing either Ptch1-GFP, NPC1-GFP or Ptchd1-GFP fusions. GFP expression, Shh-Fc immunostaining and DAPI. D, Quantification of Shh-Fc binding to COS7 cells (N≥103 cells) and to MEF cells (N≥40 cells).

2.4 The Ptchd1 cytoplasmic tail interacts with scaffolding proteins and the retromer complex

Ptchd1 is predicted to form a twelve pass transmembrane protein with a PDZ-binding motif at the C-terminal tail (Figure 11A). To identify proteins that may contribute to Ptchd1 localization or function we performed affinity-purifications from whole brain extracts with the 43 amino acid cytoplasmic C-terminus of Ptchd1 either constitute (WT) or lacking (ΔPDZ) the last 4 residues that contain the PDZ-binding motif. As a negative control, we used a protein containing an extracellular sequence of Ptchd1 (ECD, see Figure 11A, B).

Proteins retained on hexa-histidine-GST-fusions of these baits were identified by shot-gun mass-spectrometry and specificity of the interaction was assessed by comparison to the ECD control protein (Figure 11C, D; complete mass-spec data online in supplementary *Figure 5-1*). Quantitative analysis identified a number of proteins that were enriched on the wild-type C-terminus whereas other candidate binding partners were enriched on both, wild-type and ΔPDZ tails. Twelve out of thirteen proteins preferentially recovered on the wild-type Ptchd1 tail compared to the ΔPDZ mutant contained PDZ-domains, including common components of the postsynaptic density (Dlg1,2,3,4, Magi1,3, Lin7).

Interestingly, we recovered three components of the retromer complex involved in regulating dendritic protein trafficking between endosomal compartments and the plasma membrane (Choy et al., 2014): Sorting-nexin 27 (which contains a PDZ domain) was recovered selectively on the wild-type Ptchd1 tail and VPS26B and VPS35 which interacted with both the wild-type and the ΔPDZ tail.

In addition, there was a notable number of ribosomal proteins recovered both on wild-type and ΔPDZ bait proteins (RL5, 7, 8, 18A, 27, 31, 32,37, Rpl31). Whether these ribosomal proteins represent physiological binding partners or whether they are non-specifically recruited through the stretch of highly charged amino acids in the Ptchd1 cytoplasmic tail remains to be explored.

Using Western blotting, we validated our mass spectrometry approach confirming the binding of Dgl4 (also known as PSD95) and VPS35 to the recombinant Ptchd1 C-terminus. Thus, endogenous DLG4 and VPS35 from membrane and soluble mouse brain fractions were specifically recovered on the GST-fusion proteins containing the cytoplasmic but not the extracellular, negative control sequences of Ptchd1 (Figure 11E). Notably, binding of DLG4 was dependent on the PDZ-binding motif in Ptchd1 whereas VPS35 binding was not (Figure 11E).

Considering the association with post-synaptic density proteins and retromer, we tested whether endogenous Ptchd1 protein is concentrated in postsynaptic density-preparations from mouse brain. Synaptosome fractionations revealed an enrichment of Ptchd1 in the PSD obtained from adult mouse brain (Figure 11F, *Ptchd1*$^{-/y}$ brains were analyzed to control for antibody specificity). These results demonstrate a biochemical interaction of Ptchd1 with postsynaptic trafficking proteins in the mouse brain.

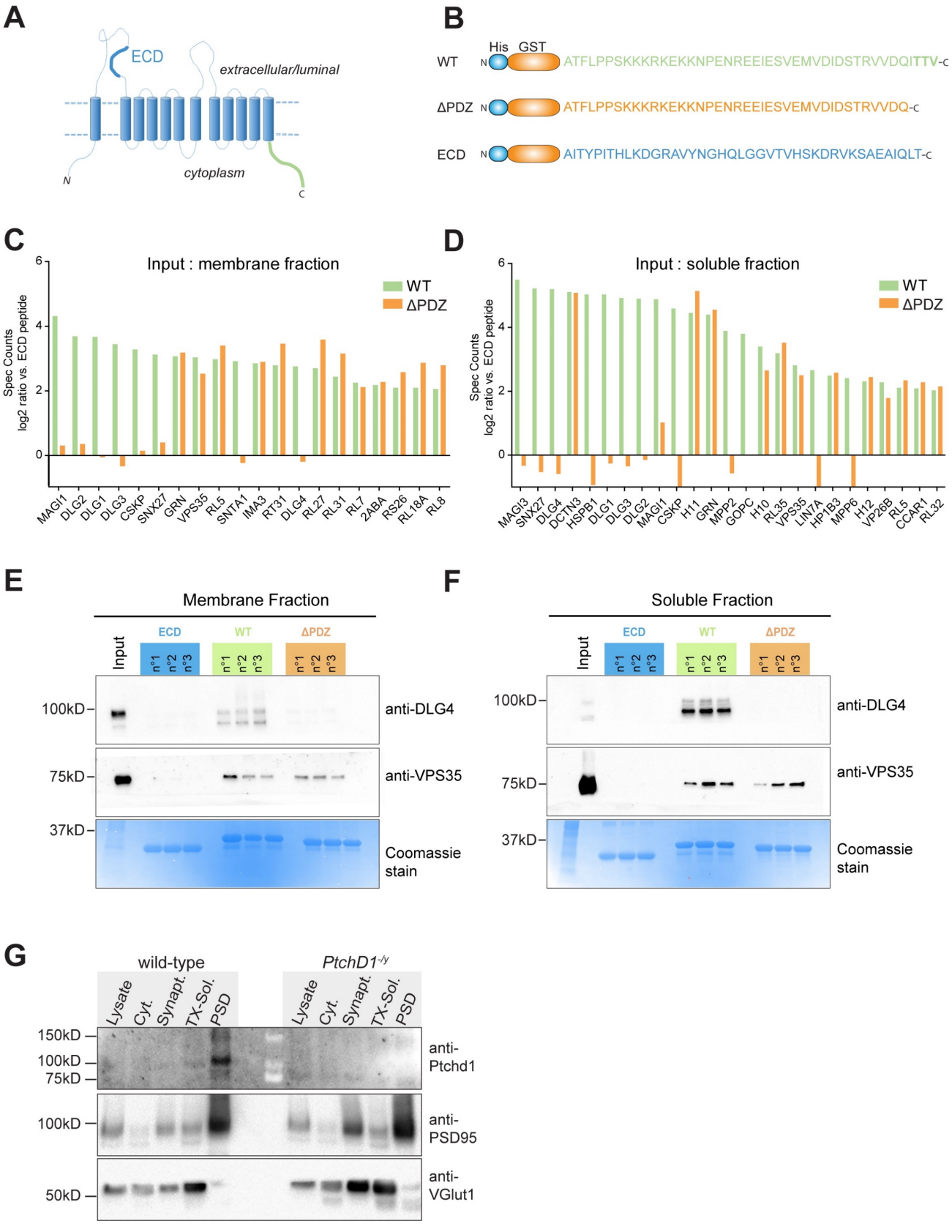
A
ECD
extracellular/luminal
cytoplasm
N
C
B
His GST
WT N ATFLPPSKKKRKEKKNPENREEIESVEMVDIDSTRVVDQITTV-C
ΔPDZ N ATFLPPSKKKRKEKKNPENREEIESVEMVDIDSTRVVDQ-C
ECD N AITYPITHLKDGRAVYNGHQLGGVTVHSKDRVKSAEAIQLT-C
C
Input : membrane fraction
WT
ΔPDZ
Spec Counts
log2 ratio vs. ECD peptide
MAGI1 DLG2 DLG1 DLG3 CSKP SNX27 GRN VPS35 RL5 SNTA1 IMA3 RT31 DLG4 RL27 RL31 RL7 2ABA RS26 RL18A RL8
D
Input : soluble fraction
WT
ΔPDZ
Spec Counts
log2 ratio vs. ECD peptide
MAGI3 SNX27 DLG4 DCTN3 HSPB1 DLG1 DLG3 DLG2 MAGI1 CSKP H11 GRN MPP2 GOPC H10 RL35 VPS35 LIN7A HP1B3 MPP6 H12 VP26B RL5 CCAR1 RL32
E
Membrane Fraction
Input
ECD
WT
ΔPDZ
n°1 n°2 n°3
100kD
75kD
37kD
anti-DLG4
anti-VPS35
Coomassie stain
F
Soluble Fraction
Input
ECD
WT
ΔPDZ
n°1 n°2 n°3
100kD
75kD
37kD
anti-DLG4
anti-VPS35
Coomassie stain
G
wild-type
PtchD1-/y
Lysate
Cyt.
Synapt.
TX-Sol.
PSD
150kD
100kD
75kD
100kD
50kD
anti-Ptchd1
anti-PSD95
anti-VGlut1

Figure 11. Ptchd1 cytoplasmic tail interacts with scaffolding proteins and retromer complex.
A, Schematic representation of predicted Ptchd1 protein topology. **B**, Three recombinant hexahistidin-glutathion-S-transferase (Joubert et al.) fusion proteins used for the pull-down analysis: WT: Ptchd1 C-terminal sequence (Pinto et al.), ΔPDZ: C-terminal lacking the predicted PDZ binding motif (orange), and ECD: negative control sequence from the first extracellular loop of the Ptchd1 (blue). **C**, Quantitative shotgun mass spectrometry data of proteins recovered in Ptchd1 pull-down assays using a soluble brain membrane fraction as input. **D**, Quantitative shotgun mass spectrometry data of proteins recovered in Ptchd1 pull-down assays using a soluble brain protein fraction as input. All proteins identified with at least 3 peptides, 400 spectra counts, and enriched at least 4-fold on the wild-type Ptchd1 bait as compared to the negative control (His-GST-ECD) are displayed. The graphs show enrichment (log2 ratio) compared to the ECD fraction (n=3 purifications, each measured in duplicate). The complete data from the mass-spec analysis is shown in the extended data Figure 5-1 (*online version*). **E,F** Validation of Ptchd1-DLG4 (PSD95) and Ptchd1-VPS35 interaction by western blotting. Ptchd1 interacting proteins were isolated by GST pull-down with ECD, WT and ΔPDZ baits from adult mouse membrane fractions or soluble brain protein extracts. The lower panel shows the respective protein fractions of the pull-down assay labeled with Coomassie dye. **G**, Synaptosome preparation from WT and *Ptchd1*$^{-/y}$ brains probed with Ptchd1, Dlg4/PSD95, and vGlut1 antibodies. 20 µg of total protein analyzed from total lysate, cytosolic, synaptosome, TritonX-100 soluble synaptosome and TritonX-100 insoluble synaptosome (PSD) fractions. Molecular weight markers are indicated in kDa.

2.5 Loss of Ptchd1 disrupts synaptic transmission in the dentate gyrus

Given the high expression of Ptchd1 in dentate granule cells and its association with the post-synaptic density proteins we tested whether the density and differentiation of glutamatergic spine synapses might be altered in the hippocampus of *Ptchd1*$^{-/y}$ mice. Dentate granule cells in perfusion-fixed tissue from adult and P21 *Ptchd1*$^{-/y}$ mice were labeled by diolistics (Gan et al., 2000), then spine density and morphology were assessed (Figure 12A, B). Using this approach, we did not detect any difference in the overall density of dendritic protrusions in *Ptchd1*$^{-/y}$ neurons (Figure 12B). Further, the fraction of headed, spine-like protrusions was unaltered (Figure 12B). Thus, Ptchd1 is dispensable for the formation of dendritic spines in dentate granule cells at P21 and in adult mice.

To determine if Ptchd1 enrichment in dentate granule cells is associated with synaptic dysfunction, we examined synaptic transmission using whole-cell recordings in acute hippocampal slices from P21-24 mice. Excitatory and inhibitory postsynaptic currents (EPSCs and IPSCs) were evoked by stimulation of the perforant pathway (Figure 12C). Interestingly, *Ptchd1*$^{-/y}$ dentate granule cells exhibited a profound reduction in the excitation/inhibition ratio (Figure 12D). AMPAR:NMDAR ratios and paired-pulse ratios of evoked glutamatergic transmission were unchanged (Figure 12E,F).

We hypothesized that the reduced excitation/inhibition ratio may be caused by an increase in inhibition or a decrease in excitation, thus we examined basal activity by measuring spontaneous EPSCs or IPSCs. Surprisingly, we observed a significant increase in the frequency of both spontaneous excitatory and inhibitory events in *Ptchd1*$^{-/y}$ dentate granule cells (Figure 12G,H). Together, these data suggest that loss of Ptchd1 results in severe alterations in synaptic function in the dentate gyrus.

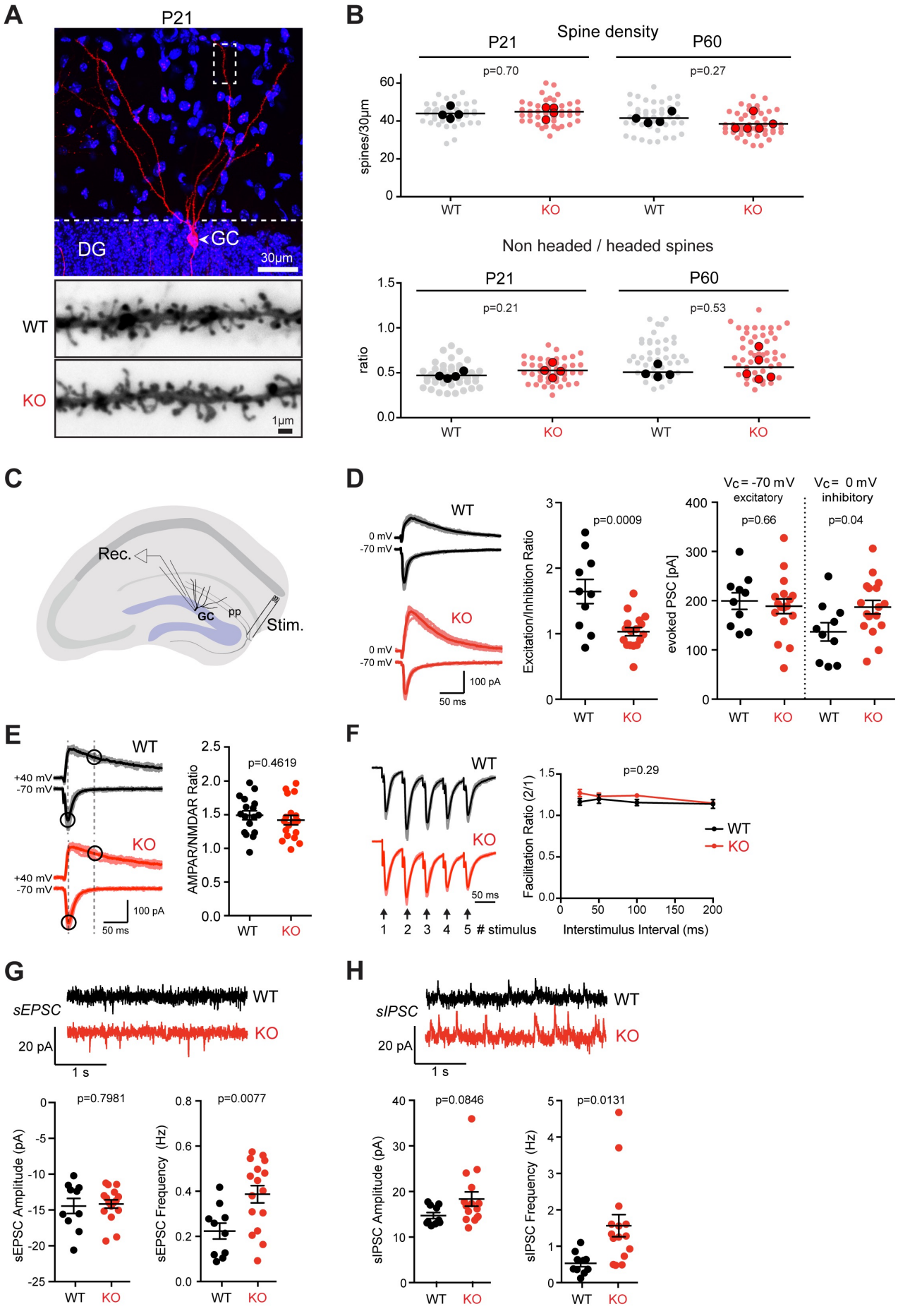
A
P21
DG
GC
30μm
WT
KO
1μm
B
Spine density
P21
P60
p=0.70
p=0.27
spines/30μm
WT
KO
Non headed / headed spines
p=0.21
p=0.53
ratio
C
Rec.
GC
pp
Stim.
D
WT
KO
0 mV
-70 mV
100 pA
50 ms
Excitation/Inhibition Ratio
p=0.0009
Vc= -70 mV
excitatory
Vc= 0 mV
inhibitory
p=0.66
p=0.04
evoked PSC [pA]
E
+40 mV
-70 mV
AMPAR/NMDAR Ratio
p=0.4619
F
p=0.29
Facilitation Ratio (2/1)
1 2 3 4 5 # stimulus
Interstimulus Interval (ms)
G
sEPSC
20 pA
1 s
p=0.7981
p=0.0077
sEPSC Amplitude (pA)
sEPSC Frequency (Hz)
H
sIPSC
p=0.0846
p=0.0131
sIPSC Amplitude (pA)
sIPSC Frequency (Hz)

Figure 12. Morphology and physiology of dentate gyrus granule cells in Ptchd1$^{-/y}$ mice.

A, Diolistic labeling (red) of a hippocampal dentate granule cell in a P21 Ptchd1$^{-/y}$ (KO) mouse (DAPI labeling of nuclei in blue). The lower panels show an example of a P21 WT and KO DG granule cell distal dendrite. B, Spine density (per 30 µm dendrite segment) and morphology (headed versus non-headed spines) were quantified for P21 and adult (P60) wild-type and *Ptchd1*$^{-/y}$ (KO) mice. Means of 4 WT and 4 *Ptchd1*$^{-/y}$ (P21) and 4 WT and 5 *Ptchd1*$^{-/y}$ (P60) mice are displayed (lines and solid dots); mean and unpaired Student t-test. The light dots represent values for individual dendritic segments scored (P21: *Ptchd1*$^{-/y}$ n=44, WT n=44; P60: *Ptchd1*$^{-/y}$ n=49, WT n=42). C, The schematic shows the configuration of whole-cell voltage-clamp recordings made from acute hippocampal slices of P21-P24 mice. Postsynaptic responses in granule cell (GC) neurons were measured following stimulation of the perforant pathway (pp). D, Representative traces of evoked EPSCs and IPSCs recorded from granule cells in acute hippocampal slices show disrupted excitation/inhibition balance in *Ptchd1*$^{-/y}$ (KO), granule cells (WT, n=10; KO, n=17; N=3 animals for each genotype; mean and SEM, unpaired *t* test). E Representative traces of evoked EPSCs used to calculate AMPAR/NMDAR ratios (WT, n=17; KO, n=18; N=3 animals for each genotype, unpaired *t* test) F, Normalized evoked postsynaptic responses of WT or *Ptchd1*$^{-/y}$ GC neurons to five stimuli delivered to the pp with a 50 inter-stimulus interval, The facilitation ratio of the 2nd EPSC amplitude normalized to the 1st EPSC amplitude shows normal facilitation across various inter-stimulus intervals in *Ptchd1*$^{-/y}$ (KO) GC neurons (Stimulus: 3rd/1st, p=0.18; 4th/1st, p=0.43; 5th/1st, p=0.64; WT, n=8; KO, n=16; N=3 animals for each genotype, two-way repeated measures ANOVA with multiple comparisons). G, Representative traces of spontaneous EPSCs from wild-type or *Ptchd1*$^{-/y}$ GC neurons which were voltage-clamped at –70 mV, sEPSC frequency (WT, 0.22±0.04 Hz; KO, 0.39±0.04 Hz) but not sEPSC amplitude (WT, 0.22±0.04 Hz; KO, 0.39±0.04 Hz) is increased in *Ptchd1*$^{-/y}$ GC neurons (WT, n=10; KO, n=16; N=3 animals for each genotype, unpaired *t* test). H, Representative traces of spontaneous IPSCs from wild-type or *Ptchd1*$^{-/y}$ GC neurons which were voltage-clamped at 0 mV., sIPSC frequency (WT, 0.53±0.09 Hz; KO, 1.56±0.3 Hz) but not sIPSC amplitudes (WT, 14.72±0.67 pA; KO, 18.35±1.57) is significantly increased in *Ptchd1*$^{-/y}$ GC neurons (WT, n=10; KO, n=15; N=3 animals for each genotype, unpaired *t* test).

2.6 Ptchd1$^{-/y}$ mice show deficits in hippocampus-related behavioral tasks

Considering the alterations in synaptic transmission we further explored behavioral phenotypes in our new line of Ptchd1 knock-out mice. In open field tests, *Ptchd1*$^{-/y}$ mice covered the same distance as littermate controls, however, the mutants frequently exhibited bouts of high mobility, largely due to jumping behaviors (Figure 13B). We then used an object recognition test, which in part depends on hippocampal function (Cohen and Stackman, 2015). Animals are exposed to novel and familiar objects in a test arena. The time exploring the objects is scored 1hr and 24 hrs after the initial exposure. While wild-type mice showed a clear preference for novel over familiar objects we observed a marked loss of short term (1hr) and long-term (24hr) memory in *Ptchd1*$^{-/y}$ mice (Figure 13C). Notably, the mean object interaction time during the first (acquisition) trial was the same for wild-type and mutant mice (Figure 13D). During the re-test, wild-type mice showed decreased interaction with the familiar object and preference for the novel object. By contrast, *Ptchd1*$^{-/y}$ mice did not exhibit significant habituation to the familiar object in the 1 hr or 24 hr re-test (Figure 13D), thus, resulting in a lack of discrimination of novel and familiar stimuli. These results indicate a cognitive deficit in this line of *Ptchd1*$^{-/y}$ mice.

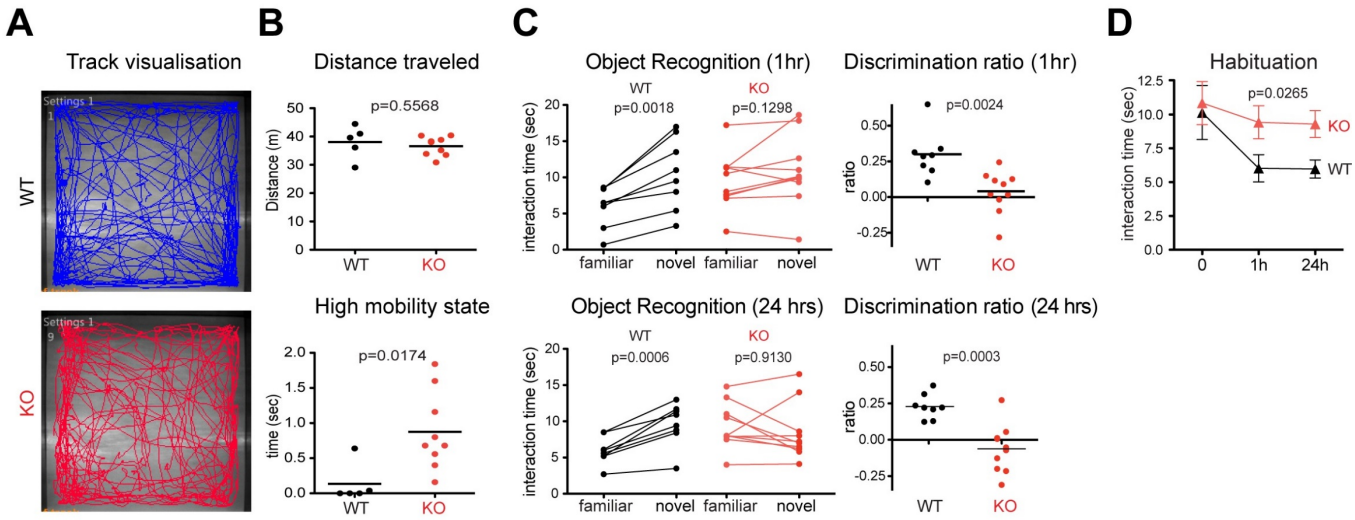

Figure 13. **Ptchd1$^{-/y}$ mouse behavioral analysis.** **A**, Open field track visualization of a KO and a WT mouse. **B**, Distance traveled in the open field arena and high mobility state (N=9 *Ptchd1*$^{-/y}$, N=5 WT), mean, unpaired t-test. **C**, Interaction time and discrimination ratio between familiar object and novel object presented 1hr and 24h after initial exposure (N=10 *Ptchd1*$^{-/y}$ N=8 WT), paired t-test. **D**, Habituation curve to familiar object over time (N=10 *Ptchd1*$^{-/y}$, N=8 WT), mean and SEM, two-way ANOVA.

2.7 Preliminary result: Ptchd1-/y mice show alterations in brain lipid homeostasis

Our work suggests that Ptchd1 is not a Shh receptor despite sequence homologies with Ptch. As described previously, Ptchd1 and the cholesterol transporter NPC1 also share sterol sensing domains. NPC1 dysfunction causes lysosomal cholesterol accumulation resulting in a severe neurodegenerative disorder. Thus, we hypothesized that Ptchd1 may be involved in lipid homeostasis and explored potential lipid alterations in *Ptchd1*$^{-/y}$ mice using an unbiased lipidomic approach. This work was done recently in collaboration with Howard Riezman's laboratory, University of Geneva. The cerebellar tissue was chosen for the analysis as it shows highest Ptchd1 expression (Figure 7) . Lipids were isolated from KO and WT cerebellum and quantified using mass spectrometry. As shown on Figure 14A a number of lipids are significantly either down or upregulated in KO animals (red dots). Glycerophospholipids (GPLs) show the most important alteration (Figure 14B), including glycerophospho-serine (PS) / -ethanolamine (PE) / -choline (PC). Interestingly, three lyso-glycerophospho-serine (lyso-PS) isoforms, metabolic intermediates of PS, are among the most downregulated lipids whereas PS (with six isoforms) are significantly upregulated. This differential alteration in the PS synthesis pathway could suggest a potential involvement of Ptchd1 in the biosynthesis or degradation of PS. Two other families of lipids are significantly down regulated: Ceramides (CMs) (nine isoforms downregulated out of fourteen detected) and sphingomyelins (SMs). This result suggest a potential involvement of Ptchd1 in lipid homeostasis however more samples and replications are under analysis to consolidate this promising finding.

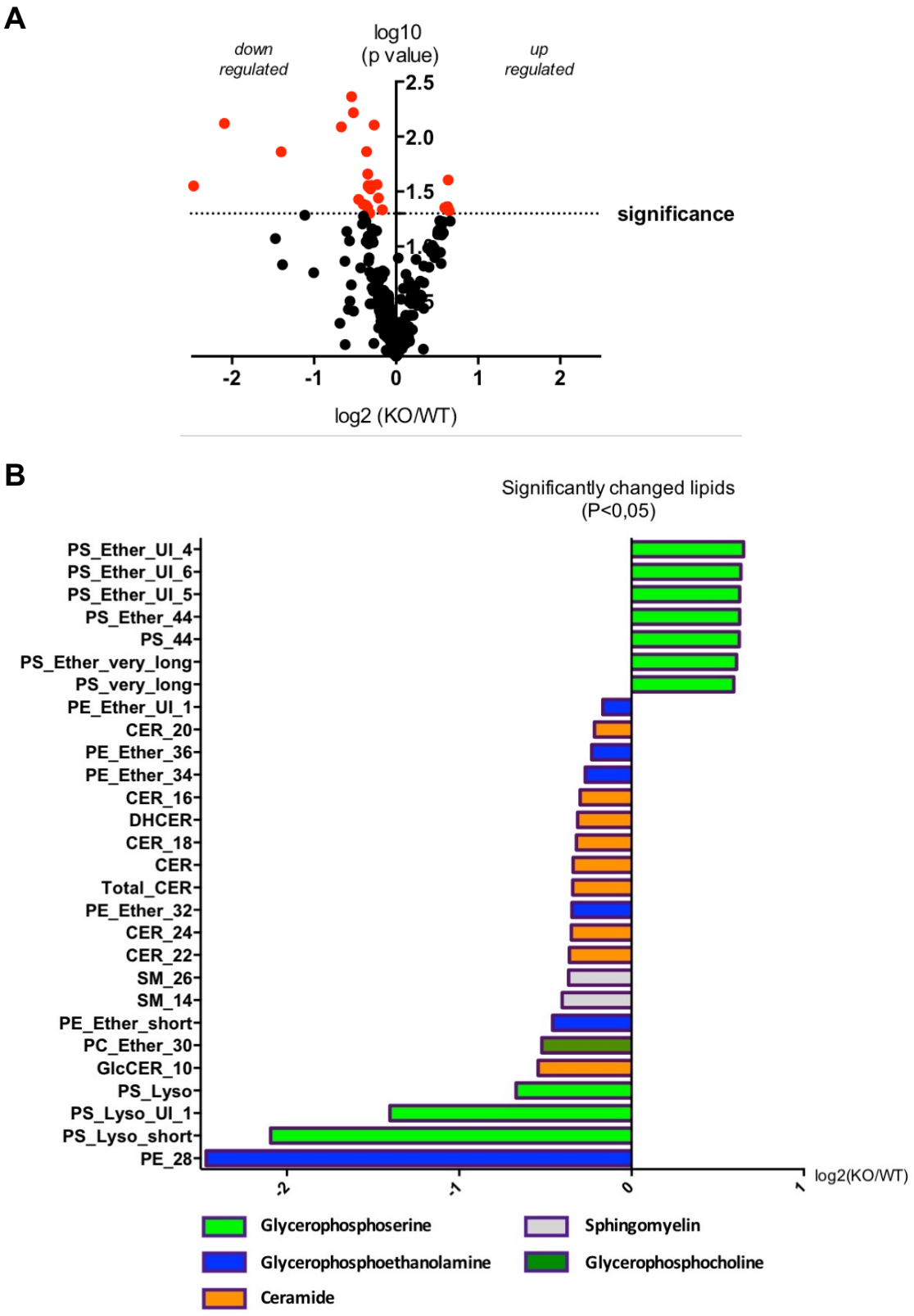

Figure 14. Brain lipid changes in *Ptchd1*$^{-/y}$ mice. A, overall view of lipid changes in KO over WT mice, significant changes are shown in red (log10(p<0.05)); (N=4 *Ptchd1*$^{-/y}$ N=4 WT), paired t-test. B, Significantly changed lipids in KO samples (p<0,05). Different lipid classes, including their metabolic intermediates, are color coded as shown at the bottom of the graph. (N=4 *Ptchd1*$^{-/y}$ N=4 WT), paired t-test.

3. Discussion

3.1 Loss-of-function experiments do not support a role in sonic-hedgehog signaling

In this study, we generated and characterized a new Ptchd1 knock-out mouse line to explore the cellular and molecular functions of the Ptchd1 protein. An important goal of our work was testing whether loss of Ptchd1 results in Shh signaling-related phenotypes *in vivo*. The hypothesis that Ptchd1 acts as a Shh receptor is based on the presence of a sterol-sensing domain and reporter assays where exogenous Ptchd1 was overexpressed (Noor et al., 2010).

A major function for Shh-Ptch1 signaling in the postnatal brain is the control of neuronal precursor proliferation in the developing cerebellum, in developing dentate granule cells and in adult neural precursors in the dentate gyrus. Thus, we tested precursor proliferation and maintenance in the hippocampal dentate gyrus and the external germinal layer of the cerebellum. However, we did not observe significant changes in Ptchd1 mutants. It is possible that the presence of Ptch1 compensates for a loss of Ptchd1, thus, obscuring a potential phenotype.

We consider this unlikely for the following reasons: (1) Heterozygous deletion of Ptch1 results in precursor over-proliferation and medulloblastomas in the mouse cerebellum, indicating that even partial loss of Ptch1-signaling results in severe Shh-related phenotypes. (Andersen and Koeppe) We did not observe binding of recombinant Shh to Ptchd1 under conditions where an interaction with Ptch1 was readily detectable. Notably, Ptchd1-like proteins are also found in non-mammalian species, including C.elegans which do not encode recognizable Shh orthologues in their genomes (Consortium, 1998). Thus, we favor the interpretation that Ptchd1 has different, Shh-independent functions in the developing and adult mouse brain.

3.2 Ptchd1 binding partners support a role in the retromer trafficking complex

Our unbiased proteomic approach identified PDZ-domain containing scaffolding molecules including synaptic scaffolding proteins. This was expected due to the C-terminal

consensus sequence –ITTV for PDZ domain interactions. In addition, we discovered an unexpected interaction with the retromer complex consisting of VPS35, VPS26B and SNX27.

Notably, SNX27 contains a PDZ-domain and its interaction depends on the C-terminal PDZ-binding motif of Ptchd1. However, VPS35 and VPS26B were also recovered on the ΔPDZ bait protein, highlighting multiple interactions sites for Ptchd1 and the retromer complex. SNX27 as well as VPS35 have been implicated in membrane protein trafficking between dendritic endosomes and the plasma membrane, in particular postsynaptic glutamate receptors and β-adrenergic receptors (Wang et al., 2013; Choy et al., 2014). Thus, retromer may be involved in trafficking of Ptchd1 between endosomal and cell surface compartments including the postsynaptic compartment.

3.3 Synaptic alterations in Ptchd1$^{-/y}$ mice

Supporting a link to synaptic trafficking proteins, we observed a critical role of Ptchd1 to the excitatory/inhibitory balance in dentate granule cells. The frequency of spontaneous excitatory as well as inhibitory events in dentate granule cells was increased. Previous work by Wells et al. (2016) demonstrated alterations in SK channel activity in somatostatin-positive interneurons in the thalamus. Thus, the alterations in spontaneous excitatory and inhibitory events in the dentate gyrus may result from Ptchd1-dependent phenotypes in glutamatergic as well as GABAergic interneurons. Dissecting the cellular and/or synaptic source of this electrophysiological phenotype will require conditional ablation of Ptchd1 from specific cell populations in the dentate gyrus.

In *Ptchd1*$^{-/y}$ dentate gyrus we did not observe alterations in facilitation ratios at glutamatergic synapses or loss of postsynaptic spine structures. This was surprising, as a recent report indicated a 33% reduction in excitatory synapse density in *Ptchd1*$^{-/y}$ hippocampus (Ung et al., 2017). One difference in our study is the focus on dentate granule cells which express the highest level of *Ptchd1* mRNA in the hippocampus. By contrast Ung et al. focused on the CA region which according to our expression analysis expresses only very low levels of Ptchd1 transcripts. Another difference between the studies is the mutant allele employed. Similar to Wells et al. (Wells et al., 2016) we used a germline deletion of exon 2. Ung et al. used a mutant allele where exon 2 is replaced with a gene trap cassette (Ung et al.,

2017). However, we consider it more likely that there is a differential requirement for Ptchd1 in synapse development across cell types with high and low Ptchd1 expression levels such as dentate granule and CA1 cells. Moreover, some phenotypes may emerge as secondary effects due to functional alterations in upstream circuit elements. Analysis of conditional mutants may resolve this in the future. As the endogenous subcellular localization of Ptchd1 is still uncertain (due to the lack of good tools), it remains unclear whether the synaptic deficits are a consequence of Ptchd1 requirement directly at the synapse or rather in endosomes trafficking (as suggested by the pull-down assay).

3.4 Behavioral alterations in Ptchd1$^{-/y}$ mice

A survey of 23 subjects with *PTCHD1* mutations reported intellectual disability, ASD, and motor alterations as phenotypes that are shared across significant sub-groups of these patients (Chaudhry et al., 2015). Moreover, several patients exhibit ADHD and hyperactivity. The increase in high mobility bouts and jumping of our *Ptchd1*$^{-/y}$ mice observed in open field assays is reminiscent of the hyperactivity phenotype reported previously for additional mouse models (Wells et al., 2016; Ung et al., 2017). Conditional ablation of *Ptchd1* in somatostatin-positive interneurons replicates the ADHD and hyperactivity phenotype of the mice but did not replicate learning deficits seen for global knock-out mice in an inhibitory avoidance task (Wells et al., 2016). The defect in objection recognition memory identified in our mouse line highlights a further cognitive deficit in this rodent model. Future work aims to illuminate whether this defect is due to hippocampal dysfunction. Taken together our work suggests that behavioral deficits in *Ptchd1*$^{-/y}$ mice are likely to be independent of changes in neuronal precursor proliferation or cell fate but rather alterations in post-mitotic neurons including deficits in synaptic transmission.

3.5 Contribution of Ptchd1 to lipid homeostasis

In addition to the Patched family, Ptchd1 also shares a conserved SSD domain with a number of protein families implicated in lipid homeostasis (Figure 6), one of the most phylogenetically similar protein to Ptchd1 is NPC1. In addition of causing cholesterol accumulation in lysosomal compartments, NPC1 deficient cells also show alterations in a

number of other lipid classes including glycerophospholipids and SMs (Lloyd-Evans et al., 2008; Tharkeshwar et al., 2017). GPLs are the most abundant lipid class in mammalian cells, present intracellular as well as plasma membranes. Cholesterol and SMs are enriched at the plasma membrane and contribute to the formation of domains that can affect the signaling and distribution of membrane proteins (Coskun and Simons, 2010). Similarly, even if less abundant, CMs are thought to be important modulators of cell signaling (Hannun and Obeid, 2008).

Our preliminary data indicates that several GPLs are down regulated in *Ptchd1*$^{-/y}$ animals including PE, PC and PS precursors. Intriguingly, PS are upregulated in *Ptchd1*$^{-/y}$ brains whereas lyso-PS, metabolic intermediates of PS, are among the most downregulated lipids. Cholesterol levels in KO samples trend towards a downregulation (data not shown) but significance was not reached due to high variability across samples (more samples are under analysis to consolidate the data).

The lipidomic approach appears to be an excellent tool to detect overall brain lipid dysregulations, however due to heterogeneity of altered lipids it remains unclear whether one class of lipid is specifically altered in *Ptchd1*$^{-/y}$ mice and leads to the alteration of others or if several lipids are affected directly by the absence of Ptchd1. The biosynthesis of different lipid classes can dependent on one another, for example PCs are precursors of PE and PS. Also, most lipids are synthesized in the endoplasmic reticulum (Fagone and Jackowski, 2009) and transported via similar pathways, mostly by endosomal/lysosomal transport. Thereby, if an alteration occur in one class of lipid it can trigger a cascade of alterations in other lipids, either directly with the lack of metabolic precursors or indirectly by affecting the entire lipid transport machinery.

In addition, the integrity of the plasma membrane is important for the function of certain ion channels (Dart, 2010). Neuronal plasma membranes includes lipid micro-domains (also called “raft”) enriched with cholesterol and sphingolipids. These lipid rafts are suggested to regulate ion channels kinetics in neurons either directly through lipid-channel interaction (Jiao et al., 2008; Fantini and Barrantes, 2009) or indirectly through the rafts physical properties influencing channel surface expression and trafficking (Andersen and Koeppe,

2007). Given that Wells et al. (2016) reported alteration in SK channel in TRN interneurons of *Ptchd1*$^{-/y}$ mice, one interpretation to their observation could be that the dysfunction of SK channels is a consequence of lipid homeostasis modification in *Ptchd1*$^{-/y}$ animals.

Also, it remains puzzling how sterols sensed by the SSD of Ptchd1 would regulated other classes of lipids. As suggested by the retromer proteins (VPS35/VPS26) recovered on the cytoplasmic tail of Ptchd1, the protein is likely to localize, at least transiently, in endosomal membranes. Endosomes are important effectors of the lipid turn-over machinery (Holthuis and Levine, 2005). Thus, if Ptchd1 acts as a sterol sensor and/or transporter, its absence may lead to sterol mislocalization and potentially create an endosomal lipid imbalance leading to the alteration of other lipids homeostasis. More targeted experiments aim to illuminate what subcellular compartments and machinery are affected. If lipid deficits are confirmed by future work, dietary and pharmacological strategies could be considered for ameliorating lipid alterations in Ptchd1 deficient patients.

4. Future directions

4.1 Is Ptchd1 part of the retromer trafficking complex ?

Our unbiased proteomic analysis of Ptchd1 binding partners revealed interactions with three components of the retromer pathway: VPS35/VPS26 and SNX27. The retromer complex recycles endocytosed protein form endosomes to the plasma membrane or to the trans golgi network (TGN) (Seaman, 2012). However, SNX27 was shown to mediate retromer trafficking of cargoes from endosomes to the plasma membrane rather than the TGN in mammalian cells (Temkin et al., 2011). In addition, the retromer complex have been recently implicated in the trafficking of dendritic endosomes and the plasma membrane, in particular postsynaptic glutamate receptors and β-adrenergic receptors (Wang et al., 2013; Choy et al., 2014). Given these lines of research, one hypothesis would be that Ptchd1 is being transported via the retromer pathway between endosomes and the plasma membrane.

Knowing in what subcellular compartment Ptchd1 localizes would greatly contribute to interpret its link with the retromer. Unfortunately, due to the lack of good tools, the sub-cellular localization of Ptchd1 remains unclear. However, considerable efforts are ongoing to generate an efficient tool to visualize the protein; the aim is to generate a mouse line expressing a fluorescently tagged Ptchd1 (split-NeonGreen line) suitable for live imaging studies (see Appendix 6.1).. The live tracking of Ptchd1 would help understand the dynamic distribution of Ptchd1 in cells, especially in neurons. This could be combined with co-localization assays using antibodies against VPS35/26, SNX27, endosomal markers (Rab5, Rab7) and lysosomal markers (Lamp1). Identifying in which cell compartment Ptchd1 localizes is an essential step to understand its molecular function.

Alternatively, given the binding of Ptchd1 with retromer components, the absence of the protein in KO mice could alter the retromer pathway. One key aspect of the retromer pathway is the internalization of plasma membrane proteins into early endosomes, then further processed in late endosomes and lysosomes (Seaman, 2012). Several methods can be used for live imaging endosomal processing. One well established method is the incorporation of lipophilic fluorescent dyes (FM-dye) to cell culture media. Due to their lipophilic properties, the FM-dyes will incorporate into plasma membranes and internalized in endosomes, allowing the visualization of endosomal trafficking by fluorescent microscopy. Alternatively, some

endocytic tracers target specifically subpopulation of endosomes (early and late) or lysosomes. A widely used method is the usage of fluorescent pH sensitive probes conjugated to dextran. Early endosomes have a pH in the range of pH 6.8-6.1, late endosomes in the range of pH 6.0-4.8 and lysosomes around pH 4.5; certain probes emit fluorescence only in a specific pH ranges and can be used to label specifically sub-population of endosomes or lysosomes (Tharkeshwar et al., 2017). These well-established assays could be used in *Ptchd1*$^{-/y}$ neuronal cultures to assess whether or not the endosomal trafficking is perturbed in the absence of Ptchd1. Overall, given the potential implication of Ptchd1 in lipid homeostasis, it is not excluded that Ptchd1 transports or senses lipids via the retromer pathway. Future work aims to confirm lipid deficits observed in *Ptchd1*$^{-/y}$ animals and assess whether or not this deficit is dependent on retromer trafficking.

4.2 Is Ptchd1 involved in lipid trafficking ?

Our unbiased lipidomic approach suggests lipid homeostasis alterations in *Ptchd1*$^{-/y}$ mice but more work is needed to understand the dysfunctions at a sub-cellular level. As previously discussed, Ptchd1 shares an SSD with the cholesterol transporter NPC1. Thus, the first aim is to image cholesterol trafficking to ask whether Ptchd1 deficient cells have either an accumulation, downregulation or mislocalization of intracellular cholesterol. Filipin staining is a well described method used to visualize cholesterol (Gimpl, 2010). Filipin is a naturally fluorescent polyene that binds to free cholesterol. We aim to use *Ptchd1*$^{-/y}$ cerebellar cultured cells to image cholesterol with filipin staining. As cerebellar granule neurons have a very small condensed cytoplasm and dense dendritic arborization, they are not suitable for cholesterol visualization and quantification. To bypass that issue, we aim to use *Ptchd1*$^{-/y}$ cerebellar astrocytes. Our preliminary fluorescent *in situ* data (not shown) suggest that astrocytes express *Ptchd1* mRNA; similarly, brain transcriptome database from Zhang et al. (2014) indicate that *Ptchd1* is significantly expressed in human and mouse glial cells. In addition, astrocytes have a big and flat cytoplasm suitable for subcellular localization studies. Thus, we aim to image and quantify cholesterol with filipin staining in *Ptchd1*$^{-/y}$ and WT cultured astrocytes.

An alternative method to image cholesterol trafficking is the incorporation of fluorescent cholesterol analogs such as dehydroergosterol (DHE)-, cholestatrienol (CTL)- or bora-diaza-indacene (BODIPY)- cholesterol. Due to their lipophilic properties, these fluorescent analogs incorporate into cells and can be used for live cell imaging. Live imaging has the advantage of monitoring cholesterol trafficking dynamically overtime and not only at a given time point.

Biosynthetic sterol trafficking can also be quantified in isolated sub-cellular compartments. Typically, radioactive cholesterol precursors (acetate or mevalonate) are incorporated in cells and the radiolabel incorporation into cholesterol is measured after sub-cellular fractionation and lipid extraction (Gimpl, 2010). However, this method remains indirect and only provides enrichment of different sub-cellular membrane compartments.

A recent method established by Tharkeshwar et al. (2017) used superparamagnetic iron oxide nanoparticles (SPIONs) to specifically isolate subcellular compartments and measure membrane lipid composition. In brief, SPIONs have an inorganic magnetic core and an organic/inorganic shell. When the shell coated with aminolipids, the SPIONs remain adhered to the plasma membrane, whereas when coated with dimercaptosuccinic acid, SPIONs are targeted to late endosomes and lysosomes. The different cellular compartments are then magnetically isolated, providing a highly specific segregation between plasma membrane and late endosomes/lysosomes. Following the isolation procedure, the different compartments can be used for lipidomic and proteomic profiling. This would be an attractive method to further characterize the lipid deficits observed in *Ptchd1*$^{-/y}$ mice.

5. Material and methods

5.1 Mice

Ptchd1 mutant mice were generated in C57BL/6N background in collaboration with the Mouse Biology Project at the University of California Davis. Targeting vector PRPGS00100_C_H03 (KOMP) was electroporated into *JM8.N4* ES cell and colonies selected. The targeting cassette is based on the knock-out first vector design, replacing exon 2 of the *Ptchd1* gene. Mice with germline transmission were mated with ROSA26-Flpe females (Jax stock no: 003946), backcrossed over ten generations with C57BL/6N mice, to remove FRT-flanked genetrap/LacZ sequences, yielding a conditional allele. Germline ablation of exon 2 was created by crossing with CMV-cre mice (Jax stock no: 006054). The "knock-out first" mice generated by the Mouse Biology Project were deposited at the MMRRC repository. Genotyping of the knock-out mice was done as follows: The $Ptchd1^{-/y}$ allele was detected by PCR using primers 5'-AACACCATGACTGAAGCAACTTGGG-3'(CSD-Ptchd1-F) with 5'-AGTGCTGAGGAGTTAGCTATGCAGG-3'(CSD-Ptchd1-R). The $Ptchd1^{WT}$ allele was detected using 5'-AACACCATGACTGAAGCAACTTGGG-3'(CSD-Ptchd1-F) with 5'-TCCAGAACTGAGAAATCAGGTTCGC-3'(CSD-Ptchd1-ttR). Only male mice were used for all experiments. Procedures related to animal experimentation were reviewed and approved by the Kantonales Veterinäramt Basel-Stadt.

5.2 In situ hybridization, PCR analysis

In situ hybridizations with chromogenic detection were done using digoxigenin labelled cRNA probes and were performed as previously described (Schaeren-Wiemers and Gerfin-Moser, 1993). The DNA fragment encoding the Ptchd1 probe contained SP6 and T7 promoters flanking the 5'- or 3'-end, respectively, *Ptchd1*:

CCGCTCTGCTCTAGGATGCTGCGGCAGGTTCTGCACAGGGGCTTGAGGACGTGTTTCTCCCGGCTTG
GCCACTTCATTGCCAGTCACCCGGTCTTCTTTGCTTCGGCGCCGGTGCTCATCTCCATCCTGCTCGGCG
CCAGCTTCAGCCGCTACCAGGTCGAAGAGAGCGTGGAGCACCTGCTGGCGCCCCAGCACAGCCTAG
CCAAGATCGAGCGCAACCTAGTCAACAGCCTCTTCCCGGTCAACCGCTCCAAGCACCGGCTCTACTCG
GACCTGCAGACCCCTGGGCGCTACGGCCGGGTCATTGTCACCTCCTACCAGAAAGCCAACATGCTAG
ACCAACATCACACGGACCTGA

Templates for in vitro transcription using SP6-polymerase (anti-sense probe) or T7-polymerase (sense probe) were amplified by PCR using ISP-SP6-5' (5'-CTATCGATTTAGGTGACACTATAGAAG-3') and ISP-T7-3' (5'-GAATTGTAATACGACTCACTATAGGGA-3') primers.

Fluorescent in situ hybridization was performed following the RNAscope Multiplex Fluorescent Assay protocol (Wang et al., 2012). The assay was performed on 20µm snap frozen P21 brain cryostat sections. Sections were cut between Bregma -1.46 and -2.40 including the dorsal hippocampus. *Ptchd1* transcripts were detected with a commercial *Ptchd1* probe (ACD, Cat No. 489651). A negative control probe (ACD, Cat No. 320871) was used to assess the specificity of hybridization signals observed. In situ images were acquired on a Widefield Axio Scan Z1 slide scanner.

For qPCR analysis, brain tissues were dissected in ice cold PBS, microdissected hippocampal sub-regions were isolated according to the protocol of Hagihara (Hagihara et al., 2009). Tissue was homogenized in Trizol (Tri Reagent, SIGMA), followed by addition of Chloroform. After homogenization, sample were centrifuged for 15min at 16'000xg. The supernatant was used for RNA purification with the RNAeasy mini plus kit (Qiagen) following manufacturer's instructions. 1µg of total RNA was reverse transcribed using random hexamers and ImProm-II Reverse Transcriptase (Promega). Quantitative RT-PCR was performed on a StepOne plus qPCR system (Applied Biosystems): Gene expression assays were done with the Power SYBR Green Master Mix (Applied Biosystems) and the comparative C_T method. cDNA levels were normalized to the house keeping gene *Gapdh* cDNA. Primer sequences used with Power SYBR Green PCR Mastermix were as follows:

Ptchd1: 5'-CAAGATCGAGCGCAACCTAG-3' and 5'-ATGTTGGCTTTCTGGTAGGAG-3'

Gapdh : 5'-CTCGTGTGGATTTGGAGAG-3' and 5'-AGTTCTCGAACTTCCTCCT-3'

Hprt: 5'-GATGAACCAGGTATGACCTAGATTTG-3' and 5'-ATGGCCTCCCATCTCCTTCAT -3'

TDO2: 5'-ATGAGTGGGTGCCCGTTTG-3' and 5'-GGCTCTGTTTACACCAGTTTGAG-3'

DSP: 5'-GCTGAAGAACACTCTAGCCCA-3' and 5'-ACTGCTGTTTCCTCTGAGACA-3'

Mrg1b: 5'-CTGGCGAGATCACGATGACG-3' and 5'-AAGCTACGCTGTTGTCTAACC-3'

Primers used to confirm *Ptchd1* exon 2 deletion were:

Forward primer in Exon1: 5'-CCAACATGCTAGACCAACATCACA-3'
Reverse primer in Exon3: 5'-TTTATGGTTCCAGCCTTGTGTTCA-3'

5.3 Antibodies, cDNA expression vectors, western blots

Polyclonal anti-Ptchd1 antibodies were raised in guinea pigs using synthetic peptides derived from the following Ptchd1 sequences: DFQKTSRVSERYLVT and VDIDSTRVVDQITTV. Peptides were conjugated to keyhole limpet hemocyanin (Eurogentec, Belgium). Anti-sera and affinity purified antibodies were tested on Western blot applications; immunohistochemical applications were inconclusive. For Western Blots the following commercial antibodies were used: mouse anti-actin (JLA20-S, DSHB) 1:3000, mouse anti-GFP (abcam, ab38689) 1:500 Mouse anti-PSD95(DLG4) (NeuroMab, 75-028) 1:3000, rabbit anti-VPS35 (Bethyl, A304-727A) 1:200, mouse anti-vGlut1 (NeuroMab, 75-066) 1:3000. For immunohistochemistry assays the following antibodies were used: rat anti-BrdU (Abcam, ab6326) 1:50 and rabbit anti-Phospho Histone 3 (PH3) (Millipore, 06-570) 1:1000

Immunoblotting was done with HRP-conjugated secondary antibodies (Jackson immunoresearch) and Pierce ECL Western blotting substrate. Signals were acquired using a digital imager (Bio-Rad, ChemiDoc MP Imaging System). The pEGFP-C1-Ptchd1 vector used for overexpression assays was created with the following cDNA: MG219209 from OriGene.

5.4 BrdU incorporation assays and diolistic labeling.

Postnatal day 4 (P4) *Ptchd1*$^{-/y}$ males and littermate wild-type controls were weighed, then injected intraperitoneally with 100mg/kg Bromodeoxyuridine (BrdU). After 30 minutes, mice were sacrificed, brains were transferred to fixative (4% paraformaldehyde, 30% Sucrose in PBS) and incubated overnight at 4°C. On the next day, brains were frozen at -80°C and 30µm cryosections were cut for immunohistochemistry. For the adult neurogenesis assay, P60 *Ptchd1*$^{-/y}$ males and wild-type littermate controls were used and analyzed 4 days after injection of BrdU. Sections underwent an antigen retrieval step before the standard immunostaining protocol: in brief, sections were wash 3 times in PBS, put 0.1% TritonX-100 in PBS for 20min, transferred to 2M HCl for 20min at 37°C, neutralized with borate buffer (0.1M,

pH=8.5) 3 times for 10 min and washed in PBS 3 times for 10 min. Then a standard immunostaining protocol was applied for BrdU and PH3 detection. Quantitative assessment of BrdU-positive cells was performed as previously described (Han et al., 2008; Li et al., 2013). Briefly, confocal image stacks were acquired from consecutive sagittal sections of cerebellum lobule VI and dorsal dentate gyrus. An anatomically equivalent block of 300 - 400 µm thickness was analyzed for each animal (10-15 30µm anatomical sections per mouse, with each section imaged as a confocal image stack). For the adult neurogenesis experiment the neurogenic sub-granular zone of the dentate gyrus was analyzed for BrdU- and PH3-positive cells. For the P4 developmental hippocampus experiment the entire DG area was analyzed.

The diolistic labeling (Gan et al., 2000) was performed according to a published protocol (Staffend and Meisel, 2011). Images were acquired on an inverted LSM700 confocal microscope (Zeiss) using 10x, 20× or 63x Apochromat objectives and controlled by Zen 2010 software. For spine counting, confocal image stacks were acquired of granule cell dendritic segments in the distal molecular layer of the dorsal dentate gyrus. Spines were counted per 30µm dendritic segment by evaluating the three-dimensional information of the image stacks. Headed and non-headed spines were distinguished manually. Images for display were assembled using Adobe Photoshop and Illustrator software. All quantitative assessments were performed by an investigator blinded to the genotype.

5.5 Sonic hedgehog binding assay

We modified a protocol from Cheng and Flanagan (Cheng and Flanagan, 2001). In brief, 12 mm glass coverslips were coated with 100 µg/ml Poly-L-lysine (Sigma) for 2 h, and then washed twice with water. MEF or COS7 cells were plated on uncoated or PLL-coated 12 mm glass coverslips respectively, in 24-well plates. Cells were transfected with either pEGFP-C1-Ptch1 + Casp9-DN-HA (HA-tagged dominant negative caspase 9, to prevent apoptosis) (Mille et al., 2009), pEGFP-C1-Ptchd1, or pEGFP-C1-NPC1, using Lipofectamine 3000 according to the manufacturer's instructions. 48 h later, the media was removed and the cells washed twice with Binding Buffer A (BBA: DMEM + 10% FBS + 0.1% NaN_2 + 50 mM HEPES). 500 nM Shh-Fc, diluted in BBA, was then added to the cells and incubated for 1 h at room temperature. Cells were then washed once in BBA, then three times in PBS (containing Ca^{2+} and Mg^{2+}), followed

by fixation with 4% PFA for 10 minutes at room temperature. Shh-Fc was detected with standard immunostaining protocols using Cy3-conjugated donkey anti-human-Fc, diluted 1:1000 in PBS with 1% normal donkey serum and 0.1% Triton X-100, for 1.5 h at room temperature. The coverslips were imaged on a Leica DM6B microscope with a Hammamatsu Orca Flash 4.0 camera, using Leica LASX software. Shh-Fc binding to Ptch-expressing cells results in a distinct cell surface staining pattern. The percentage of cells exhibiting binding was scored by an investigator blinded to the identity of the transfected cDNA. The assay was conducted three times, twice with COS7 cells and once with mouse embryonic fibroblast cells yielding similar results. Surface expression of overexpressed proteins was confirmed by surface biotinylation and revealed similar surface levels of Ptch and Ptchd1 proteins.

5.6 Biochemical interaction assays

cDNA encoding fusion peptide sequences used for pull-down analysis were inserted in frame in a pET9d-His6-GST vector. Plasmids were transformed in BL21 Rosetta *E. coli*. Bacteria were grown to reach OD=0.8. Expression was induced with 200µM IPTG for 2.5 hours at 25°C. Bacteria were pelleted at 5'000 x g at 4°C for 20 min, lysed and purified on Protino Ni-TED 2000 columns (Machery-Nagel). Purified proteins were dialyzed overnight at 4°C against storage buffer (PBS, 2mM EDTA, 10% Glycerol, 0.1mM AEBSF, 0.1mM TCEP). For affinity purification of binding partners, Ptchd1 peptides were bound to Glutathione Sepharose 4 fast flow beads (GE Healthcare, #17-5132-01) following the manufacturer's instructions. For the input fractions: adult male mouse brains (n=3) were lysed and homogenized in ~1.5ml/gr in an ice cold glass homogenizer and centrifuged at 800 x g at 4°C for 10min. The supernatant was transferred to a new tube and centrifuged at 16'000 x g at 4°C for 15min. The resulting supernatant was used as "Soluble fraction input", the pellet, re-suspended in lysis buffer was used as "Membrane fraction Input". GST beads were washed three times with PBS before adding the Input fractions. Beads were incubated with protein extracts for 2 hours at room temperature, then washed again three times with 0.1%TX-100 in PBS, followed by elution with 2% sodium deoxycolate in 130ul. Eluted samples were trypsin digested and prepared for mass spectrometry following standard protocol.

5.7 Mass spectrometry analysis and label-free quantification

Samples were subjected to LC–MS analysis in triplicates using a dual pressure LTQ-Orbitrap Elite mass spectrometer (Thermo Fisher Scientific) connected to an electrospray ion source (Thermo Fisher Scientific) as described (Glatter et al., 2012). Peptide separation was carried out on an EASY nLC-1000 system (Thermo Fisher Scientific) equipped with a RP-HPLC column (75 µm × 30 cm) packed in-house with C18 resin (ReproSil-Pur C18–AQ, 1.9 µm resin, Dr. Maisch GmbH). A linear gradient from 95% solvent A (0.15% formic acid, 2% acetonitrile) and 5% solvent B (98% acetonitrile, 0.15% formic acid) to 28% solvent B over 90 min at a flow rate of 0.2 µl/min was used. Data acquisition mode was set to obtain one high resolution MS scan in the FT part of the mass spectrometer at a resolution of 240,000 full widths at half-maximum (at m/z 400) followed by 20 MS/MS scans in the linear ion trap of the most intense ions (TOP20) using rapid scan speed. Unassigned and singly charged ions were excluded from analysis and dynamic exclusion duration was set to 30 s.
MS1-based label-free quantification of MS data was performed using Progenesis QI software (Nonlinear Dynamics (Waters), version 2.0).

MS raw files were imported into Progenesis QI software and analyzed using the default parameter settings. MS/MS-data were exported from the software in “mgf” format and searched with a target/decoy strategy against a database containing forward and reverse sequences of the proteome from Mus musculus (UniProt, 33,984 entries) using MASCOT (version 2.4.1). Search criteria required full tryptic specificity allowing for three missed cleavages. Carbamidomethylation of cysteine was specified in Mascot as a fixed modification. Oxidation of methionine and acetyl of the N-terminus were specified in Mascot as variable modifications. Mass tolerance was set to 10 ppm for precursor ions and 0.6 Da for fragment ions. The peptide and protein false discovery rate (FDR) was set to 1%. Results from the database search were imported into Progenesis QI and the resulting peptide measurement list containing peak area values of identified peptides was exported. Processing and statistical evaluation of peptide and protein quantities between samples was performed using SafeQuant (Glatter et al., 2012). Normalized peptide and protein intensities from SafeQuant analysis were used to calculate intensity ratios, log2 ratios and q values between experimental conditions for identified proteins.

5.8 Synaptosome preparation

Adult male mouse brain was homogenized with a glass homogenizer in 20µl/mg tissue 0.32M Sucrose, 1mM $NaHCO_3$, 1mM $MgCl_2$, 0,5mM $CaCl_2$ and complete EDTA-free protease inhibitor (Roche Applied Science). The homogenate was centrifuged at 1'400 x g for 10 min. The supernatant was further centrifuged at 16'000 x g for 20 min at 4°C resulting in the crude synaptosomal pellet and a cytosolic supernatant. The pellet was re-suspended in 1 mM $NaHCO_3$, 0.32 M sucrose and loaded on top of a sucrose step gradient (1 M, 1.2 M sucrose) and centrifuged at 82'500 x g for 2 h. Synaptosomes were collected at the interface between the 1.0 M and 1.2 M sucrose layers. The synaptosome fraction was extracted for 15 min at 4 °C in 25 mM Tris-HCl pH 8.1, 0.32 M sucrose, 1 % Triton X-100 and centrifuged at 32,800 x g for 30 min to yield a Triton X-100 soluble and insoluble (PSD) fraction.

5.9 Mouse behavior analysis.

Behavioral testing was done as previously described (Leger et al., 2013; Nguyen et al., 2016). We used wild-type littermate control and *Ptchd1*$^{-/y}$ male mice aged between 7 and 9 weeks. Behavioral tests were done on three mouse cohorts (total n=10 *Ptchd1*$^{-/y}$, n=8 wild-type littermate). Mice were first tested in an open field arena (50x50×25 cm) and then the object recognition test was initiated on the following day in the same arena. Before each behavioral test, mice were allowed to habituate to the behavioral room for at least 30 min. After each testing, the arena and objects were cleaned with 70% ethanol. Explorative behavior in the open field was recorded for 7 mins with a BASLER Ethovision Camera (Noldus). The distance traveled and mobility state were quantified using Ethovision 10 software (Noldus). The user-defined thresholds for definition of the high mobility state was set to 60% of changed pixel area. The open field test served as a habituation phase for the novel object recognition test. For the novel object recognition test, recordings were acquired with a Canon camera (LEGRIA HFG10).

Animals were allowed to explore two identical small Falcon tissue culture flasks (50 ml volume) filled with sand for 5 min. Then mice were returned to their home cage. After a 1 hr inter-trial interval, one flask was replaced with a tower of Lego bricks and duration of

interaction was assessed in a second 5 min trial. Exploration time for each object was measured manually by an investigator blinded to the genotype of the mouse. If a mouse exhibited less than 3 s exploring one object during the initial exposure, it was excluded from the analysis (this was the case for 2 KO animals). Object exploration was defined as the orientation of the mouse snout toward the object, sniffing or touching with the snout within 2 cm distance. Leaning, climbing, looking over or biting the objects were not considered as exploration time. The position of the objects in the test was counterbalanced between the animals in a group.

5.10 Electrophysiology

Horizontal hippocampal slices (300 µm) were prepared from both hemispheres of age-matched mice (P21-24) anesthetized with intraperitoneal injection of ketamine/xylazine (100mg/kg and 10mg/kg, respectively). Mice were transcardially perfused with an ice-cold oxygenated (95% O_2/5% CO_2) NMDG-based dissection buffer (Ting et al., 2014) (in mM): 93 NMDG, 93 HCl, 2.5 KCl, 1.2 NaH_2PO_4, 30 $NaHCO_3$, 25 Glucose, 20 HEPES, 5 Na-ascorbate, 3 Na-pyruvate, 2 Thiourea, 10 MgSO4, and 0.5 CaCl2, pH 7.4, 310 mOsm. Slices were cut with a vibratome (VT1200S, Leica, Buffalo Grove, IL) in oxygenated NMDG-dissection buffer. Slices were transferred to NMDG-based oxygenated dissection buffer at 32°C for 15 min and then transferred to room temperature artificial cerebrospinal fluid (ACSF; in mM): 124 NaCl, 2.5 KCl, 1.2 NaH_2PO_4, 2 $CaCl_2$, 2 $MgSO_4$, 24 $NaHCO_3$, 5 HEPES, and 13 glucose, pH 7.4, 310 mOsm. Slices incubated at room temperature at least one hour to allow for recovery, then transferred to the recording chamber and perfused (1.5–2.0 ml/min) with oxygenated ACSF at room temperature.

Somatic whole-cell recordings were made from granule cells in the dentate gyrus, which were voltage clamped with a Multiclamp 700B amplifier (Molecular Devices, Sunnyvale, CA) and identified using infrared-differential interference contrast video microscopy, digitized by Digidata 1440a (Molecular Devices). Patch pipettes (4–8 MΩ) were filled with voltage clamp (V_c) solution for paired-pulse facilitation, Excitation/Inhibition ratio, and sEPSC/sIPSC, experiments (in mM): V_c = 135 $CsMeSO_3$, 10 HEPES, 8 NaCl, 0.3 EGTA, 4 Mg-ATP, 0.3 Na-GTP,

5 QX-314 and 0.1 spermine, 295 mOsm. We measured excitatory postsynaptic currents by voltage-clamping granule cells to -70 mV, near the reversal potential for inhibition.

Inhibitory postsynaptic currents were measured by voltage-clamping granule cells to 0 mV, near the reversal potential for excitation. Data were filtered at 2 kHz, digitized at 10 kHz, and analyzed with Clampfit 10.6 (Molecular Devices). Perforant path (pp) afferents were stimulated with a small glass bipolar electrode (Master-9 and ISO-Flex Stimulator, A.M.P.I., Jerusalem, Israel). Short-term facilitation was induced with five stimuli of equal intensity presented at variable interstimulus intervals, ranging from 25 ms to 200 ms. Peak amplitudes measured from the responses from stimulations delivered at various frequencies were quantified and normalized to the first peak amplitude in a train. Responses from at least ten sweeps for each stimulation frequency were quantified to generate the facilitation ratios.

AMPAR/NMDAR ratios were recorded in the presence of 10 µM Bicuculline (Tocris). The average of the maximal peak from ten evoked EPSCs voltage clamped at -70mV and the average of the maximal peak of ten evoked EPSCs voltage-clamped +40mV (50ms following the maximal peak recorded at -70mV) were used to quantify AMPAR/NMDAR ratios. 2.5 minutes of recorded granule cell neurons voltage-clamped at -70mV for sEPSC and 0 mV for sIPSC were analyzed with Axograph X software (version 1.5.4) to determine the amplitude and frequency of sEPSCs and sIPSCs. The average of the maximal peak from ten evoked EPSCs voltage clamped at -70mV and the average of the maximal peak of ten evoked EPSCs voltage-clamped at 0mV were used to quantify Excitation/Inhibition ratios.

5.11 Lipid Extraction

Similarly to (Guri et al., 2017), lipid extraction was performed using a modified MTBE protocol. Briefly, cerebellar samples from 21 days old mice (n=4 WT; n=4 KO) were extracted and immediately snap-frozen in liquid nitrogen. Subsequently, tissues were pulverized into a fine powder in an in-house-constructed metal mortar, pre-cooled on dry ice. Of that, 30-35 mg ground liver tissue was weighed in a pre-chilled 2 mL Eppendorf Safe-Lock tube and resuspended in 100 mlH2O and transferred into a 2 mL Eppendorf tube. Then, 360 ml methanol was added and vortexed. A mixture of lipid standards (see Key Resources Table)

plus 50 ml 1.4 mm Zirconium glass beads (Bertin Technologies, France) were added and the pulverized tissue was homogenized using a Cryolysis System (Bertin Technologies, France) (program: 6200-3x45-045) cooled to 4°C. MTBE (1.2 mL) was then added and the sample was incubated for one hr at room temperature with shaking (750 rpm). Phase separation was induced by adding 200 mlH2O. After 10 min of incubation at RT, the sample was centrifuged at 1000 x g for 10 min (RT). The upper (organic) phase was transferred in a 13 mm screw cap glass tube and the lower phase was extracted with 400 ml artificial upper phase (MTBE/methanol/water (10:3:1.5, v/v)). The two upper phases were combined and the total lipid extract was divided in 3 equal aliquots (one for phospholipids (TL), one for sterols (S) in 2 mL amber vials and one for sphingolipid

(SL) detection in a 13 mm glass tube) and dried in a Centrivap at 50°C or under a nitrogen flow. The TL and S aliquots were ready to be analyzed by mass spectrometry and were kept at -80°C. The SL aliquot was deacylated to eliminate phospholipids by methylamine treatment (Clarke method). 0.5 mL monomethylamine reagent (MeOH/H2O/n-butanol/Methylamine solution (4:3:1:5 v/v) was added to the dried lipid, followed by sonication (5 min). Samples were then mixed and incubated for one hr at 53°C and dried (as above). The monomethylamine treated lipids were desalted by n-butanol extraction. 300 mlH2O saturated n-butanol was added to the dried lipids. The sample was vortexed, sonicated for 5 min and 150 ml MS grade water was added. The mixture was vortexed thoroughly and centrifuged at 3200 x g for 10 min. The upper phase was transferred in a 2 mL amber vial. The lower phase was extracted twice more with 300 mlH2O saturated n-butanol and the upper phases were combined and dried (as above).

5.12 Lipidomic analysis and quantification

Similarly to (Guri et al., 2017), phospholipid and Sphingolipid Detection were done on a Triple Quadrupole TSQ Vantage (ThermoFischer Scientific). LC-MS or HPLC grade solvents were used and the samples were pipetted in a 96 well plate (final volume = 100 ml). Positive mode solvent: Chloroform/Methanol/Water (2:7:1 v/v) + 5mM Ammonium Acetate. Negative mode solvent: Chloroform/Methanol (1:2 v/v) + 5mM Ammonium Acetate. The TL and SL aliquots were resuspended in 250 ml Chloroform/methanol (1:1 v/v) and sonicated for 5 min. The TL were diluted 1:50 in negative and positive mode solvents and the SL were diluted 1:10 in

positive mode solvent and infused onto the mass spectrometer. Tandem mass spectrometry for the identification and quantification of phospho- and sphingo-lipid molecular species was performed using multiple reaction monitoring (MRM) with a TSQ Vantage Triple Stage Quadrupole Mass Spectrometer (Thermo Fisher Scientific) equipped with a robotic nanoflow ion source, Nanomate HD (Advion Biosciences, Ithaca, NY). The collision energy was optimized for each lipid class. The detection conditions for each lipid class are listed below. Ceramide species were also quantified with a loss of water in the first quadrupole. Each biological replicate was read in 2 technical replicates (TR). Each TR comprised 3 measurements for each transition. Lipid concentrations were calculated relative to the relevant internal standards and then normalized to the total phosphate content of each total lipid extract, as described in (Ding et al., 2013). Data was then normalized to age-matched control

5.13 Statistical analysis and experimental design

Statistical analysis was done with Prism software (GraphPad software). Images from immunohistochemical and dye labeling experiments were analyzed in Fiji (Image J) with manual cell or spine counting. Sample sizes are chosen based on previous examples from the literature, and variation observed in the experiment. Exclusion criteria were animal weight which differed from the population mean by at least 20% or severe behavioral alterations observed in single animals before the experiment. No animals were excluded in the present study. Blinding was applied as stated for each experimental procedure below.

The qRT-PCR analysis was performed with n=3 mouse brain tissues for each time point and brain area. Data was analyzed with multiple comparison one-way ANOVA test. P values (Tukey's multiple comparison test) are shown in Figure 1E.

The FISH *in situ* quantification was done with N=3 WT mice; n=22 hippocampi (11 coronal sections with 6 to 8 hippocampi per animal).

The developmental BrdU analysis was performed with N=5 mice per genotype (for EGL , n= 65 *Ptchd1*$^{-/y}$, 61 WT sections; for the hippocampal study n= 61 *Ptchd1*$^{-/y}$, 61 WT sections). Cells positive for either BrdU or PH3 were normalized to the EGL area. The P4 hippocampal

analysis was normalized to the dentate gyrus area. Cell densities assessed per section were averaged per animal and genotype differences analyzed with an unpaired t-test using the number of animals as "N". P-values are shown in Figure 3 B and D.

The adult neurogenesis analysis was done with N=5 mice per genotype (n=78 *Ptchd1*$^{-/y}$ sections; n=80 WT sections). All BrdU/PH3 scoring was done blinded to genotype. Cells in the sub-granular zone positive for either BrdU or PH3 were normalized to the length of the sub-granular zone. Sections were averaged per animal and genotype differences were analyzed with an unpaired t-test, p-values are shown in Figure 4B. Shh-Fc binding quantification was analyzed on N≥103 COS7 cells and N≥40 MEF cells.

In the diolistic experiments, image acquisition and spine counting analysis was done by an investigator blinded to genotype, for P21 N=4 *Ptchd1*$^{-/y}$ and N=4 WT; n=44 anatomical sections per genotype, for P60 N=5 *Ptchd1*$^{-/y}$ and N=4 WT; *Ptchd1*$^{-/y}$ n=49, WT n=42 sections. Spine densities per dendritic segment were averaged per animal and genotype differences were analyzed with an Unpaired t-test, p-values are shown on Figure 6B. The open field behavioral data was obtained with automated video tracking software Ethovision 10. The data was analyzed with an unpaired t-test; p-values are shown in Figure 7.

All behavioral tests were analyzed by an investigator blinded to the genotype. For the novel object recognition test, the initial exploration time was analyzed with an unpaired t-test. Interaction times with objects A and B were analyzed with a repeated measure two-way ANOVA test. Discrimination ratios were analyzed with an unpaired t-test. The habituation time to object A was analyzed with a repeated measure two-way ANOVA test (Figure 7G).

The electrophysiological characterization was performed with n≥10 cells and N=3 mice per genotype by an investigator blinded to genotype. An unpaired t test was used to assess significance in excitation/inhibition ratios, sEPSC, and sIPSC data. A two-way repeated measures ANOVA with a Sidak's multiple comparisons test was used to assess significance in short-term plasticity experiments.

6. Appendix

6.1 Challenges to localize the Ptchd1 protein

As commercial antibodies against Ptchd1 are not available, we started the project with *in vitro* Ptchd1 over-expression assays. We used plasmids containing the Ptchd1 sequence fused with either an HA-tag or the enhanced green fluorescent protein (EGFP). In COS cells overexpressing Ptchd1-EGFP, Ptchd1 co-localizes with the ER marker calnexin (expression pattern is similar with the HA-tag and with HEK cells, data not shown). Over-expressed proteins, when not properly processed by the cell, often tend to aggregate in the ER, so it is unclear whether this pattern reflects a potential localization of Ptchd1 in the ER or if the protein is simply stuck up in the ER. Also, depending on plasmid amounts, low Ptchd1 expression was also observed at the plasma membrane. In addition, over-expression assays in neuronal cultures were inconclusive (cells died after transfection).

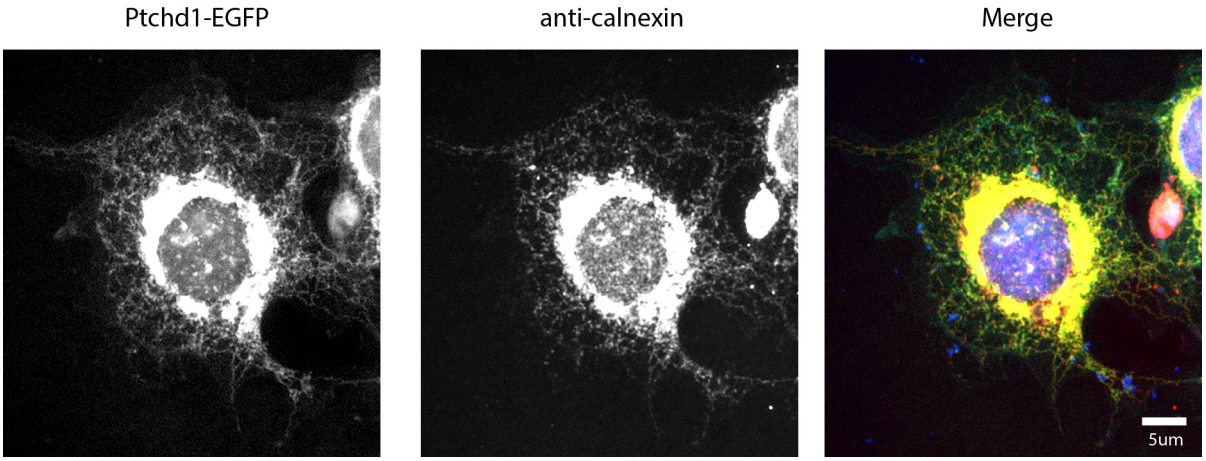

Figure 15. Ptchd1-EGFP over-expression in COS cells. Fluorescent imaging of COS cells overexpressing Ptchd1-EGFP (left). Transfected cells were immunostained with the ER marker, calnexin (middle). Merged signals show important co-localization of Ptchd1-EGFP with calnexin (Yang et al.).

In parallel, we generated several "home-made" anti-Ptchd1 antibodies raised against different parts of the protein. One antibody successfully recognized the protein in western blot assays and was used to validate the *Ptchd1*$^{-/y}$ mouse line (Figure 8). However, despite considerable effort spent generating different antibodies, none of the sera (even when purified) were suitable for immunohistochemical assays.

To circumvent the problem, a knock-in mouse line expressing a fluorescently labeled Ptchd1 is being generated. The fluorescent tag used is a modified GFP protein with more stable and stronger fluorescence called NeonGreen (NG). Similarly to Feng et al. (2017) the NG protein is split in two parts: the 11th beta-strand of NG is fused to Ptchd1 for endogenous expression and the other part of the protein (NG 1-10th) can later be transfected, electroporated or virally infected exogenously. The NG protein become fluorescent only when the two parts expressed in the cell bind covalently and irreversibly (Figure 16A). Thereby, the exogenous addition of NG 1-10th allows to sparsely label and live-track Ptchd1 in a subset of cells (with the use a specific promoters) and in a temporally controlled manner.

We used the Crispr-Cas9 genetic engineering tool to knock-in the NG 11th strand to the N-terminal sequence of Ptchd1. In brief, an exogenous single stranded DNA sequence encoding for NG-11th along with a guide RNA (gRNA) and the Cas9 enzyme are injected in mouse oocytes; the gRNA serves as a guide for the Cas9 enzyme to cut the DNA upstream from the desired PAM motif, the homology arms of the donor DNA can then anneal to the 3' cut DNA strand and thereby insert the donor DNA sequence in the mouse genome (Figure 16B). Injected oocytes are then transferred in pseudo-pregnant mice and the resulting litters are genotyped and sequenced for correct DNA insertion.

Several experiments are ongoing or planned to assess whether or not this tool efficiently labels Ptchd1. Ptchd1-NG-11th mice can be used for several localization assays. For instance, cerebellar Ptchd1-NG-11th neuronal cultures infected with a virus carrying NG 1-10th can be used for live imaging studies. Alternatively, a promoter driven virus carrying the NG 1-10th can be directly injected in Ptchd1-NG-11th mice brain allowing sparse labeling of Ptchd1 in a cell type specific manner.

A

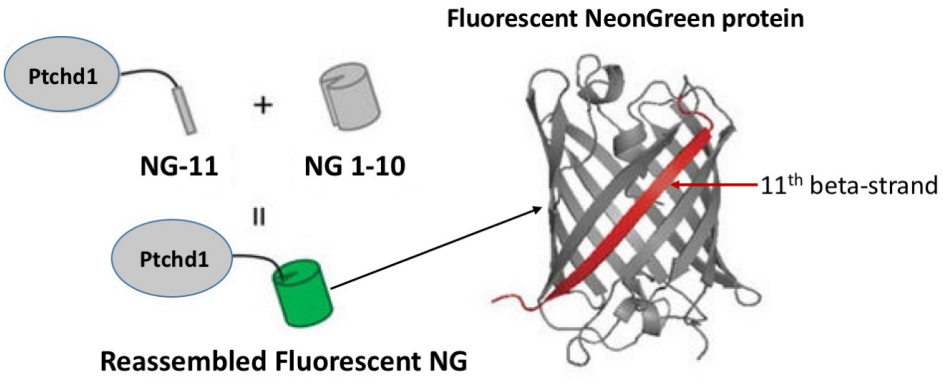

B

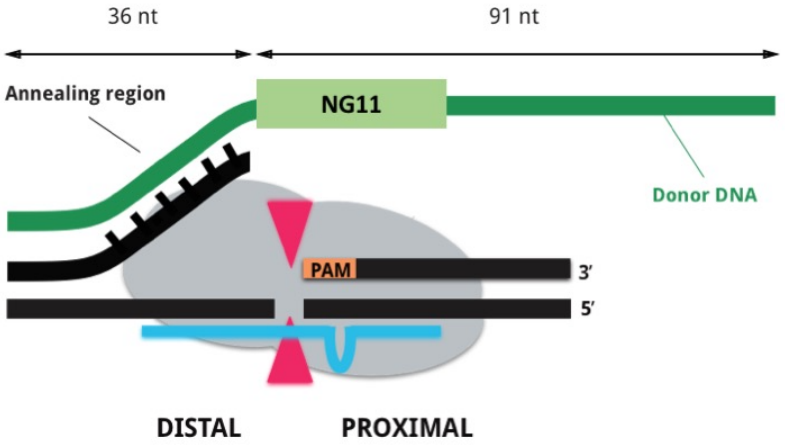

Figure 16. Ptchd1-NeonGreen mouse line engineering. A, The 11th beta strand of the NeonGreen protein (NG-11) is fused to the N-term of Ptchd1. When the NG 1-10 part of the protein is added to a cell expressing Ptchd1-NG-11, the two parts covalently bind and restore fluorescence. **B**, Genetic engineering of the NG-11 knock-in: the guide RNA (blue) guides the Cas9 enzyme (grey) to make a double stranded DNA cut (red) upstream of the selected PAM motif. The cut 3' strand will anneal to the homology arm of the single stranded donor DNA encoding for the NG-11 part. DNA repair mechanisms will insert the knock-in sequence on the complementary 5' strand.

6.2 Index of Figures

6.3 Index of Abbreviations

PTCHD1	Human Patched domain containing protein 1 (PTCHD1=human gene; *Ptchd1*=mouse gene, Ptchd1=mouse protein)
ASD	Autism spectrum disorders
ID	Intellectual disability
Shh	Sonic hedgehog
Ptch	Patched
NPC1	Niemann-pick C-1 type
DSM	Diagnostic and statistical manual of mental disorders
ICD	World Health Organization's International Statistical Classification of Diseases and Related Health Problems
PDD	Pervasive developmental disorders
E/I ratio	Excitatory over inhibitory ratio
CNV	Copy number variant
SNP	Single nucleotide polymorphism
iPSCs	Human induced pluripotent stem cells
XLID	X-chromosome linked intellectual disability
SSD	Sterol sensing domain
Smo	Smoothend
EGFP	Enhanced green fluorescent protein
P*n*	Postnatal day *n*
PH3	Phospho-histone 3
Ptchd1$^{-/y}$	Ptchd1 male hemizygous knock-out
KO	Knock-out
WT	Wild-type
EGL	External granule cell layer of the cerebellum
MEF	Mouse embryonic fibroblast
ECD	Extracellular domain/sequence
GST	Glutathione-S-transferase
PSD	Post-synaptic density
EPSC	Excitatory post-synaptic current

IPSC	Inhibitory post-synaptic current
sE/IPSCs	Spontaneous excitatory or inhibitory post-synaptic current
AMPAR	Amino-3-hydroxy-5-methyl-4isoxazolepropionic acid receptor
NMDA	N-Methyl-D-aspartic acid receptor
GPL	Glycerophospholipid
PS	Glycerophospho-serine
PE	Glycerophospho-ethanolamine
PC	Glycerophospho-choline
CM	Ceramide
SM	Sphingomyelin
TGN	Trans golgi network
SPION	Superparamagnetic iron oxide nanoparticle

7. References

Aigner S, Heckel T, Zhang JD, Andreae LC, Jagasia R (2014) Human pluripotent stem cell models of autism spectrum disorder: emerging frontiers, opportunities, and challenges towards neuronal networks in a dish. Psychopharmacology (Berl) 231:1089-1104.

Amaral DG, Schumann CM, Nordahl CW (2008) Neuroanatomy of autism. Trends Neurosci 31:137-145.

Andersen OS, Koeppe RE, 2nd (2007) Bilayer thickness and membrane protein function: an energetic perspective. Annu Rev Biophys Biomol Struct 36:107-130.

Anderson JS, Druzgal TJ, Froehlich A, DuBray MB, Lange N, Alexander AL, Abildskov T, Nielsen JA, Cariello AN, Cooperrider JR, Bigler ED, Lainhart JE (2011) Decreased interhemispheric functional connectivity in autism. Cereb Cortex 21:1134-1146.

Argos M (2015) Arsenic Exposure and Epigenetic Alterations: Recent Findings Based on the Illumina 450K DNA Methylation Array. Curr Environ Health Rep 2:137-144.

Bandim JM, Ventura LO, Miller MT, Almeida HC, Costa AE (2003) Autism and Mobius sequence: an exploratory study of children in northeastern Brazil. Arq Neuropsiquiatr 61:181-185.

Bassell GJ, Warren ST (2008) Fragile X syndrome: loss of local mRNA regulation alters synaptic development and function. Neuron 60:201-214.

Baxter AJ, Brugha TS, Erskine HE, Scheurer RW, Vos T, Scott JG (2015) The epidemiology and global burden of autism spectrum disorders. Psychol Med 45:601-613.

Berkel S, Marshall CR, Weiss B, Howe J, Roeth R, Moog U, Endris V, Roberts W, Szatmari P, Pinto D, Bonin M, Riess A, Engels H, Sprengel R, Scherer SW, Rappold GA (2010) Mutations in the SHANK2 synaptic scaffolding gene in autism spectrum disorder and mental retardation. Nat Genet 42:489-491.

Besag FM (2018) Epilepsy in patients with autism: links, risks and treatment challenges. Neuropsychiatr Dis Treat 14:1-10.

Bilder D, Pinborough-Zimmerman J, Miller J, McMahon W (2009) Prenatal, perinatal, and neonatal factors associated with autism spectrum disorders. Pediatrics 123:1293-1300.

Buchmayer S, Johansson S, Johansson A, Hultman CM, Sparen P, Cnattingius S (2009) Can association between preterm birth and autism be explained by maternal or neonatal morbidity? Pediatrics 124:e817-825.

Casanova MF, Buxhoeveden DP, Switala AE, Roy E (2002) Neuronal density and architecture (Gray Level Index) in the brains of autistic patients. J Child Neurol 17:515-521.

Casanova MF, van Kooten IA, Switala AE, van Engeland H, Heinsen H, Steinbusch HW, Hof PR, Trippe J, Stone J, Schmitz C (2006) Minicolumnar abnormalities in autism. Acta Neuropathol 112:287-303.

Chakrabarti S, Fombonne E (2005) Pervasive developmental disorders in preschool children: confirmation of high prevalence. Am J Psychiatry 162:1133-1141.

Chaudhry A et al. (2015) Phenotypic spectrum associated with PTCHD1 deletions and truncating mutations includes intellectual disability and autism spectrum disorder. Clin Genet 88:224-233.

Cheng HJ, Flanagan JG (2001) Cloning and characterization of RTK ligands using receptor-alkaline phosphatase fusion proteins. Methods Mol Biol 124:313-334.

Choi CS, Gonzales EL, Kim KC, Yang SM, Kim JW, Mabunga DF, Cheong JH, Han SH, Bahn GH, Shin CY (2016) The transgenerational inheritance of autism-like phenotypes in mice exposed to valproic acid during pregnancy. Sci Rep 6:36250.

Choy RW, Park M, Temkin P, Herring BE, Marley A, Nicoll RA, von Zastrow M (2014) Retromer mediates a discrete route of local membrane delivery to dendrites. Neuron 82:55-62.

Christensen DL, Baio J, Van Naarden Braun K, Bilder D, Charles J, Constantino JN, Daniels J, Durkin MS, Fitzgerald RT, Kurzius-Spencer M, Lee LC, Pettygrove S, Robinson C, Schulz E, Wells C, Wingate MS, Zahorodny W, Yeargin-Allsopp M, Centers for Disease C, Prevention (2016) Prevalence and Characteristics of Autism Spectrum Disorder Among Children Aged 8 Years--Autism and Developmental Disabilities Monitoring Network, 11 Sites, United States, 2012. MMWR Surveill Summ 65:1-23.

Cohen SJ, Stackman RW, Jr. (2015) Assessing rodent hippocampal involvement in the novel object recognition task. A review. Behav Brain Res 285:105-117.

Consortium CeS (1998) Genome sequence of the nematode C. elegans: a platform for investigating biology. Science (New York, NY 282:2012-2018.

Coskun U, Simons K (2010) Membrane rafting: from apical sorting to phase segregation. FEBS Lett 584:1685-1693.

Courchesne E, Pierce K (2005) Why the frontal cortex in autism might be talking only to itself: local over-connectivity but long-distance disconnection. Curr Opin Neurobiol 15:225-230.

Courchesne E, Pierce K, Schumann CM, Redcay E, Buckwalter JA, Kennedy DP, Morgan J (2007) Mapping early brain development in autism. Neuron 56:399-413.

Dart C (2010) Lipid microdomains and the regulation of ion channel function. J Physiol 588:3169-3178.

de la Torre-Ubieta L, Won H, Stein JL, Geschwind DH (2016) Advancing the understanding of autism disease mechanisms through genetics. Nat Med 22:345-361.

De Rubeis S et al. (2014) Synaptic, transcriptional and chromatin genes disrupted in autism. Nature 515:209-215.

Durand CM et al. (2007) Mutations in the gene encoding the synaptic scaffolding protein SHANK3 are associated with autism spectrum disorders. Nat Genet 39:25-27.

Ebrahimi-Fakhari D, Sahin M (2015) Autism and the synapse: emerging mechanisms and mechanism-based therapies. Curr Opin Neurol 28:91-102.

Ehninger D, Silva AJ (2011) Rapamycin for treating Tuberous sclerosis and Autism spectrum disorders. Trends Mol Med 17:78-87.

Elsabbagh M, Divan G, Koh YJ, Kim YS, Kauchali S, Marcin C, Montiel-Nava C, Patel V, Paula CS, Wang C, Yasamy MT, Fombonne E (2012) Global prevalence of autism and other pervasive developmental disorders. Autism Res 5:160-179.

Fagone P, Jackowski S (2009) Membrane phospholipid synthesis and endoplasmic reticulum function. J Lipid Res 50 Suppl:S311-316.

Fantini J, Barrantes FJ (2009) Sphingolipid/cholesterol regulation of neurotransmitter receptor conformation and function. Biochim Biophys Acta 1788:2345-2361.

Feng S, Sekine S, Pessino V, Li H, Leonetti MD, Huang B (2017) Improved split fluorescent proteins for endogenous protein labeling. Nat Commun 8:370.

Folstein S, Rutter M (1977a) Genetic influences and infantile autism. Nature 265:726-728.

Folstein S, Rutter M (1977b) Infantile autism: a genetic study of 21 twin pairs. J Child Psychol Psychiatry 18:297-321.

Fombonne E (2009) Epidemiology of pervasive developmental disorders. Pediatr Res 65:591-598.

Fombonne E, Roge B, Claverie J, Courty S, Fremolle J (1999) Microcephaly and macrocephaly in autism. J Autism Dev Disord 29:113-119.

Francis A, Msall M, Obringer E, Kelley K (2013) Children with autism spectrum disorder and epilepsy. Pediatr Ann 42:255-260.

Franklin TB, Russig H, Weiss IC, Graff J, Linder N, Michalon A, Vizi S, Mansuy IM (2010) Epigenetic transmission of the impact of early stress across generations. Biol Psychiatry 68:408-415.

Gan WB, Grutzendler J, Wong WT, Wong RO, Lichtman JW (2000) Multicolor "DiOlistic" labeling of the nervous system using lipophilic dye combinations. Neuron 27:219-225.

Garcia-Penas JJ, Dominguez-Carral J, Pereira-Bezanilla E (2012) [Abnormalities of synaptogenesis in autism. Pathogenic and therapeutic implications]. Rev Neurol 54 Suppl 1:S41-50.

Gaugler T, Klei L, Sanders SJ, Bodea CA, Goldberg AP, Lee AB, Mahajan M, Manaa D, Pawitan Y, Reichert J, Ripke S, Sandin S, Sklar P, Svantesson O, Reichenberg A, Hultman CM, Devlin B, Roeder K, Buxbaum JD (2014) Most genetic risk for autism resides with common variation. Nat Genet 46:881-885.

Geschwind DH, State MW (2015) Gene hunting in autism spectrum disorder: on the path to precision medicine. Lancet Neurol 14:1109-1120.

Ghahramani Seno MM, Kwan BY, Lee-Ng KK, Moessner R, Lionel AC, Marshall CR, Scherer SW (2011) Human PTCHD3 nulls: rare copy number and sequence variants suggest a non-essential gene. BMC Med Genet 12:45.

Gimpl G (2010) Cholesterol-protein interaction: methods and cholesterol reporter molecules. Subcell Biochem 51:1-45.

Glatter T, Ludwig C, Ahrne E, Aebersold R, Heck AJ, Schmidt A (2012) Large-scale quantitative assessment of different in-solution protein digestion protocols reveals superior cleavage efficiency of tandem Lys-C/trypsin proteolysis over trypsin digestion. Journal of proteome research 11:5145-5156.

Goodrich LV, Milenkovic L, Higgins KM, Scott MP (1997) Altered neural cell fates and medulloblastoma in mouse patched mutants. Science 277:1109-1113.

Guri Y, Colombi M, Dazert E, Hindupur SK, Roszik J, Moes S, Jenoe P, Heim MH, Riezman I, Riezman H, Hall MN (2017) mTORC2 Promotes Tumorigenesis via Lipid Synthesis. Cancer Cell 32:807-823 e812.

Habela CW, Song H, Ming GL (2016) Modeling synaptogenesis in schizophrenia and autism using human iPSC derived neurons. Mol Cell Neurosci 73:52-62.

Hagihara H, Toyama K, Yamasaki N, Miyakawa T (2009) Dissection of hippocampal dentate gyrus from adult mouse. J Vis Exp.

Han YG, Spassky N, Romaguera-Ros M, Garcia-Verdugo JM, Aguilar A, Schneider-Maunoury S, Alvarez-Buylla A (2008) Hedgehog signaling and primary cilia are required for the formation of adult neural stem cells. Nature neuroscience 11:277-284.

Hannun YA, Obeid LM (2008) Principles of bioactive lipid signalling: lessons from sphingolipids. Nat Rev Mol Cell Biol 9:139-150.

Hiilesmaa VK, Bardy AH, Granstrom ML, Teramo KA (1980) Valproic acid during pregnancy. Lancet 1:883.

Holthuis JC, Levine TP (2005) Lipid traffic: floppy drives and a superhighway. Nat Rev Mol Cell Biol 6:209-220.

Hurley AM, Tadrous M, Miller ES (2010) Thimerosal-containing vaccines and autism: a review of recent epidemiologic studies. J Pediatr Pharmacol Ther 15:173-181.

Hutsler JJ, Zhang H (2010) Increased dendritic spine densities on cortical projection neurons in autism spectrum disorders. Brain Res 1309:83-94.

Izzi L, Levesque M, Morin S, Laniel D, Wilkes BC, Mille F, Krauss RS, McMahon AP, Allen BL, Charron F (2011) Boc and Gas1 each form distinct Shh receptor complexes with Ptch1 and are required for Shh-mediated cell proliferation. Dev Cell 20:788-801.

Jamain S, Quach H, Betancur C, Rastam M, Colineaux C, Gillberg IC, Soderstrom H, Giros B, Leboyer M, Gillberg C, Bourgeron T, Paris Autism Research International Sibpair S (2003) Mutations of the X-linked genes encoding neuroligins NLGN3 and NLGN4 are associated with autism. Nat Genet 34:27-29.

Jiao J, Garg V, Yang B, Elton TS, Hu K (2008) Protein kinase C-epsilon induces caveolin-dependent internalization of vascular adenosine 5'-triphosphate-sensitive K+ channels. Hypertension 52:499-506.

Joubert BR et al. (2016) DNA Methylation in Newborns and Maternal Smoking in Pregnancy: Genome-wide Consortium Meta-analysis. Am J Hum Genet 98:680-696.

Keown CL, Shih P, Nair A, Peterson N, Mulvey ME, Muller RA (2013) Local functional overconnectivity in posterior brain regions is associated with symptom severity in autism spectrum disorders. Cell Rep 5:567-572.

Kleijer KT, Schmeisser MJ, Krueger DD, Boeckers TM, Scheiffele P, Bourgeron T, Brose N, Burbach JP (2014) Neurobiology of autism gene products: towards pathogenesis and drug targets. Psychopharmacology (Berl) 231:1037-1062.

Kolvin I (1971) Studies in the childhood psychoses. I. Diagnostic criteria and classification. Br J Psychiatry 118:381-384.

Krumm N, Turner TN, Baker C, Vives L, Mohajeri K, Witherspoon K, Raja A, Coe BP, Stessman HA, He ZX, Leal SM, Bernier R, Eichler EE (2015) Excess of rare, inherited truncating mutations in autism. Nat Genet 47:582-588.

Kuwabara PE, Labouesse M (2002) The sterol-sensing domain: multiple families, a unique role? Trends Genet 18:193-201.

Lai K, Kaspar BK, Gage FH, Schaffer DV (2003) Sonic hedgehog regulates adult neural progenitor proliferation in vitro and in vivo. Nature neuroscience 6:21-27.

Lancaster MA, Renner M, Martin CA, Wenzel D, Bicknell LS, Hurles ME, Homfray T, Penninger JM, Jackson AP, Knoblich JA (2013) Cerebral organoids model human brain development and microcephaly. Nature 501:373-379.

Leblond CS et al. (2014) Meta-analysis of SHANK Mutations in Autism Spectrum Disorders: a gradient of severity in cognitive impairments. PLoS Genet 10:e1004580.

Leger M, Quiedeville A, Bouet V, Haelewyn B, Boulouard M, Schumann-Bard P, Freret T (2013) Object recognition test in mice. Nature protocols 8:2531-2537.

Li G, Fang L, Fernandez G, Pleasure SJ (2013) The ventral hippocampus is the embryonic origin for adult neural stem cells in the dentate gyrus. Neuron 78:658-672.

Libbey JE, Sweeten TL, McMahon WM, Fujinami RS (2005) Autistic disorder and viral infections. J Neurovirol 11:1-10.

Lionel AC et al. (2013) Rare exonic deletions implicate the synaptic organizer Gephyrin (GPHN) in risk for autism, schizophrenia and seizures. Hum Mol Genet 22:2055-2066.

Lloyd-Evans E, Morgan AJ, He X, Smith DA, Elliot-Smith E, Sillence DJ, Churchill GC, Schuchman EH, Galione A, Platt FM (2008) Niemann-Pick disease type C1 is a sphingosine storage disease that causes deregulation of lysosomal calcium. Nat Med 14:1247-1255.

Lyall K, Croen L, Daniels J, Fallin MD, Ladd-Acosta C, Lee BK, Park BY, Snyder NW, Schendel D, Volk H, Windham GC, Newschaffer C (2017) The Changing Epidemiology of Autism Spectrum Disorders. Annu Rev Public Health 38:81-102.

Maglione MA, Das L, Raaen L, Smith A, Chari R, Newberry S, Shanman R, Perry T, Goetz MB, Gidengil C (2014) Safety of vaccines used for routine immunization of U.S. children: a systematic review. Pediatrics 134:325-337.

Marshall CR et al. (2008) Structural variation of chromosomes in autism spectrum disorder. Am J Hum Genet 82:477-488.

Mille F, Thibert C, Fombonne J, Rama N, Guix C, Hayashi H, Corset V, Reed JC, Mehlen P (2009) The Patched dependence receptor triggers apoptosis through a DRAL-caspase-9 complex. Nat Cell Biol 11:739-746.

Morgan JT, Chana G, Pardo CA, Achim C, Semendeferi K, Buckwalter J, Courchesne E, Everall IP (2010) Microglial activation and increased microglial density observed in the dorsolateral prefrontal cortex in autism. Biol Psychiatry 68:368-376.

Nelson SB, Valakh V (2015) Excitatory/Inhibitory Balance and Circuit Homeostasis in Autism Spectrum Disorders. Neuron 87:684-698.

Nguyen TM, Schreiner D, Xiao L, Traunmuller L, Bornmann C, Scheiffele P (2016) An alternative splicing switch shapes neurexin repertoires in principal neurons versus interneurons in the mouse hippocampus. eLife 5.

Noor A et al. (2010) Disruption at the PTCHD1 Locus on Xp22.11 in Autism spectrum disorder and intellectual disability. Sci Transl Med 2:49ra68.

Ornoy A (2009) Valproic acid in pregnancy: how much are we endangering the embryo and fetus? Reprod Toxicol 28:1-10.

Pantelis PC, Kennedy DP (2017) Deconstructing atypical eye gaze perception in autism spectrum disorder. Sci Rep 7:14990.

Pasca S (2018) Building three-dimensional human brain organoids. Nat Neurosci.

Patriarchi T, Amabile S, Frullanti E, Landucci E, Lo Rizzo C, Ariani F, Costa M, Olimpico F, J WH, F MV, Renieri A, Meloni I (2016) Imbalance of excitatory/inhibitory synaptic protein expression in iPSC-derived neurons from FOXG1(+/-) patients and in foxg1(+/-) mice. Eur J Hum Genet 24:871-880.

Pinto D et al. (2010) Functional impact of global rare copy number variation in autism spectrum disorders. Nature 466:368-372.

Postorino V, Fatta LM, Sanges V, Giovagnoli G, De Peppo L, Vicari S, Mazzone L (2016) Intellectual disability in Autism Spectrum Disorder: Investigation of prevalence in an Italian sample of children and adolescents. Res Dev Disabil 48:193-201.

Rao TS, Andrade C (2011) The MMR vaccine and autism: Sensation, refutation, retraction, and fraud. Indian J Psychiatry 53:95-96.

Rodier PM (2002) Converging evidence for brain stem injury in autism. Dev Psychopathol 14:537-557.

Ronald A, Hoekstra RA (2011) Autism spectrum disorders and autistic traits: a decade of new twin studies. Am J Med Genet B Neuropsychiatr Genet 156B:255-274.

Roullet FI, Lai JK, Foster JA (2013) In utero exposure to valproic acid and autism--a current review of clinical and animal studies. Neurotoxicol Teratol 36:47-56.

Rutter M (1972) Childhood schizophrenia reconsidered. J Autism Child Schizophr 2:315-337.

Rutter M (1979) Maternal deprivation, 1972-1978: new findings, new concepts, new approaches. Child Dev 50:283-305.

Saavedra-Rodriguez L, Feig LA (2013) Chronic social instability induces anxiety and defective social interactions across generations. Biol Psychiatry 73:44-53.

Seaman MN (2012) The retromer complex - endosomal protein recycling and beyond. J Cell Sci 125:4693-4702.

Shcheglovitov A, Shcheglovitova O, Yazawa M, Portmann T, Shu R, Sebastiano V, Krawisz A, Froehlich W, Bernstein JA, Hallmayer JF, Dolmetsch RE (2013) SHANK3 and IGF1 restore synaptic deficits in neurons from 22q13 deletion syndrome patients. Nature 503:267-271.

Skinner MK (2011) Environmental epigenetic transgenerational inheritance and somatic epigenetic mitotic stability. Epigenetics 6:838-842.

Staffend NA, Meisel RL (2011) DiOlistic labeling in fixed brain slices: phenotype, morphology, and dendritic spines. Current protocols in neuroscience / editorial board, Jacqueline N Crawley [et al] Chapter 2:Unit 2 13.

Stromland K, Nordin V, Miller M, Akerstrom B, Gillberg C (1994) Autism in thalidomide embryopathy: a population study. Dev Med Child Neurol 36:351-356.

Tang G, Gudsnuk K, Kuo SH, Cotrina ML, Rosoklija G, Sosunov A, Sonders MS, Kanter E, Castagna C, Yamamoto A, Yue Z, Arancio O, Peterson BS, Champagne F, Dwork AJ, Goldman J, Sulzer D (2014) Loss of mTOR-dependent macroautophagy causes autistic-like synaptic pruning deficits. Neuron 83:1131-1143.

Temkin P, Lauffer B, Jager S, Cimermancic P, Krogan NJ, von Zastrow M (2011) SNX27 mediates retromer tubule entry and endosome-to-plasma membrane trafficking of signalling receptors. Nat Cell Biol 13:715-721.

Tharkeshwar AK, Trekker J, Vermeire W, Pauwels J, Sannerud R, Priestman DA, Te Vruchte D, Vints K, Baatsen P, Decuypere JP, Lu H, Martin S, Vangheluwe P, Swinnen JV, Lagae L, Impens F, Platt FM, Gevaert K, Annaert W (2017) A novel approach to analyze lysosomal dysfunctions through subcellular proteomics and lipidomics: the case of NPC1 deficiency. Sci Rep 7:41408.

Ting JT, Daigle TL, Chen Q, Feng G (2014) Acute brain slice methods for adult and aging animals: application of targeted patch clamp analysis and optogenetics. Methods Mol Biol 1183:221-242.

Tora D, Gomez AM, Michaud JF, Yam PT, Charron F, Scheiffele P (2017) Cellular Functions of the Autism Risk Factor PTCHD1 in Mice. J Neurosci 37:11993-12005.

Tuchman R (2006) Autism and epilepsy: what has regression got to do with it? Epilepsy Curr 6:107-111.

Ung DC et al. (2017) Ptchd1 deficiency induces excitatory synaptic and cognitive dysfunctions in mouse. Mol Psychiatry.

Vaags AK et al. (2012) Rare deletions at the neurexin 3 locus in autism spectrum disorder. Am J Hum Genet 90:133-141.

Vargas DL, Nascimbene C, Krishnan C, Zimmerman AW, Pardo CA (2005) Neuroglial activation and neuroinflammation in the brain of patients with autism. Ann Neurol 57:67-81.

Veenstra-VanderWeele J, Blakely RD (2012) Networking in autism: leveraging genetic, biomarker and model system findings in the search for new treatments. Neuropsychopharmacology 37:196-212.

Viscidi EW, Triche EW, Pescosolido MF, McLean RL, Joseph RM, Spence SJ, Morrow EM (2013) Clinical characteristics of children with autism spectrum disorder and co-occurring epilepsy. PLoS One 8:e67797.

Wang F, Flanagan J, Su N, Wang LC, Bui S, Nielson A, Wu X, Vo HT, Ma XJ, Luo Y (2012) RNAscope: a novel in situ RNA analysis platform for formalin-fixed, paraffin-embedded tissues. J Mol Diagn 14:22-29.

Wang X et al. (2013) Loss of sorting nexin 27 contributes to excitatory synaptic dysfunction by modulating glutamate receptor recycling in Down's syndrome. Nature medicine 19:473-480.

Wechsler-Reya RJ, Scott MP (1999) Control of neuronal precursor proliferation in the cerebellum by Sonic Hedgehog. Neuron 22:103-114.

Wells MF, Wimmer RD, Schmitt LI, Feng G, Halassa MM (2016) Thalamic reticular impairment underlies attention deficit in Ptchd1(Y/-) mice. Nature 532:58-63.

Whibley AC et al. (2010) Fine-scale survey of X chromosome copy number variants and indels underlying intellectual disability. Am J Hum Genet 87:173-188.

Witter FR, Zimmerman AW, Reichmann JP, Connors SL (2009) In utero beta 2 adrenergic agonist exposure and adverse neurophysiologic and behavioral outcomes. Am J Obstet Gynecol 201:553-559.

Yang ZJ, Ellis T, Markant SL, Read TA, Kessler JD, Bourboulas M, Schuller U, Machold R, Fishell G, Rowitch DH, Wainwright BJ, Wechsler-Reya RJ (2008) Medulloblastoma can be initiated by deletion of Patched in lineage-restricted progenitors or stem cells. Cancer Cell 14:135-145.

Zhang Y, Chen K, Sloan SA, Bennett ML, Scholze AR, O'Keeffe S, Phatnani HP, Guarnieri P, Caneda C, Ruderisch N, Deng S, Liddelow SA, Zhang C, Daneman R, Maniatis T, Barres BA, Wu JQ (2014) An RNA-sequencing transcriptome and splicing database of glia, neurons, and vascular cells of the cerebral cortex. J Neurosci 34:11929-11947.

Zimmerman AW, Jyonouchi H, Comi AM, Connors SL, Milstien S, Varsou A, Heyes MP (2005) Cerebrospinal fluid and serum markers of inflammation in autism. Pediatr Neurol 33:195-201.

Acknowledgements

First, I thank my PhD advisor Peter Scheiffele for his great mentoring during my studies. His constant guidance and feedback really contributed to keep the project on track. His extensive scientific knowledge and the exciting discussions we shared really shaped my scientific thinking and as he would say: “think it through”.

I thank my committee members, Silvia Arber and Fiona Doetsch for always giving positive feedback and excellent suggestions for the project. I am also grateful to René Hen my Master internship supervisor at Columbia University; he gave me the opportunity to have an unforgettable experience abroad in one of the most renowned university worldwide. This internship really broadened my professional and personal perspectives and greatly contributed to make my doctoral studies possible.

I thank all lab members present during those four years for creating a very peaceful and nice work atmosphere, especially the PhD students who really contributed to support on one another in difficult times. I thank Caroline Bornmann, Harald Witte, Laetitia Burklé and Thi-minh Nguyen for helping and advising me when I started working in the lab. I am also very grateful to Andrea Gomez who performed the electrophysiological recording and gave excellent feedback for the project and the publication of my manuscript.

At last, I am extremely grateful to my family, friends and girlfriend who always supported me and helped me maintain a healthy life balance during these intense years.

David Tora

Address: 47, Klingentalstrasse
4057 Basel, Switzerland
Phone: +33679099964
Email : david.tora@unibas.ch

Date of Birth: 11.03.1990
Place of Birth: Strasbourg, France
Nationality: French and Hungarian

Work experience and skills

July-October 2018:

Postdoctoral fellow, Laboratory of Pr. Scheiffele, Biozentrum, University of Basel, Switzerland

- Pursuing my Ph.D. project by generating a new transgenic mouse line

October 2014-July 2018:

Ph.D. student, Laboratory of Pr. Scheiffele, Biozentrum, University of Basel, Switzerland

- Investigated the pathophysiology of autism spectrum disorders (ASD) by exploring the functions of the Patched domain containing protein 1 (PTCHD1), a risk gene associated with ASD:

- Successfully identified cellular functions of the ASD risk gene studied during my Ph.D.
- Successfully published my work as a first author in a peer reviewed journal (Journal of Neuroscience)
- Able to meet strict deadlines, weekly meetings with my supervisor to update the aims of the project
- Strategic thinking and problem-solving skills, established two new research methods currently used in the laboratory (neuron diolistic labeling and generation of "CrispR" based transgenic mice lines)
- Extended my interpersonal and management skills by teaching undergraduate students during my studies (80 hours/year) and mentored two starting Ph.D. students (for 5-6 months each)
- Rigorous training to present and communicate my work in international scientific meetings
- Developed and led my project autonomously during 4 years

January-July 2014:

Master student, New York State Psychiatric Institute, Columbia University, New York, United States (Laboratory of Pr. René Hen)

- Studied the behavioral function of adult-born neurons in the brain using optogenetic tools

- Developed a surgical method for optogenetic fibers implantation in the mammalian brain
- Improved my scientific and non-scientific vocabulary in English
- Adapted easily to a new work environment and culture

July-August 2013:

Summer student, IGBMC institute, Strasbourg, France (Laboratory of Pr. Brigitte Kieffer)

- Identification and characterization of orphan GPCRs in addictive behaviors

Career oriented trainings with certification

- **Novartis Drug discovery and development (D3) simulation course,** Basel, Switzerland, 2018
- **Good clinical practice (GCP-E6(R2) 2016)**, TRREE online, 2018
- **Project management course**, (SPOL AG), Basel, Switzerland, 20118

Academic education

2018 **Ph.D. degree in Neurobiology**, University of Basel, Switzerland
2014 **Master's degree in Neuroscience**, University of Strasbourg, France
2012 **Bachelor's degree (License) in Biology**, University of Strasbourg, France

Research trainings and presentations

- **Gordon conference on Autism spectrum disorders and Fragile-X syndrome**, Tuscany, Italy, 2018
- **CSHL training on autism spectrum disorders**, Cold Spring Harbor, United-States, 2017
- **Swiss Society for Neuroscience Annual Meeting**, Basel, Switzerland, 2016, 2017
- **LTK Module 1**, Introductory Course in Laboratory Animal Science (FELASA Category B), Basel, 2014

Publication

Cellular Functions of the Autism Risk Gene PTCHD1 in Mice. David Tora, Andrea Gomez, Jean-Francois Michaud, Patricia Yam, Frédéric Charron, Peter Scheiffele. *Journal of Neuroscience (2017).*

Languages

- **French:** Native
- **English:** Fluent, full working proficiency
- **German:** Intermediate
- **Hungarian:** Native

Informatics skills

Proficient: Word, PowerPoint, Excel, Illustrator, ImageJ, Prism

Student job experiences

2012 Reception officer and waiter, Cinemas UGC, Strasbourg, France
2009 to 2011 Bar tender/waiter, Strasbourg, France
2009 & 2010 (July) Mouse facility technician, IGBMC institute, Strasbourg, France

Extra-curricular interests

Voluntary:

- **Member of the "PhD representatives" committee**, seeking to build a community for PhD students from the life science department of the University of Basel by organizing retreats, courses and social events (link: https://phdstudents.biozentrum.unibas.ch/phd-representatives/)

- **Member of the Basel graduate consulting club,** promote the consulting industry and provide a platform for Ph.D. student interested in consulting (link: https://graduateconsultingclub.org/)

Sports and passions:

- Skiing, mountain hiking, kayaking, badminton (national level, competitions for 7 years), soccer